

PRIMARY RESEARCH

Open Access



# Identification and clinical validation of EMT-associated prognostic features based on hepatocellular carcinoma

Dafeng Xu<sup>1</sup>, Yu Wang<sup>2</sup>, Jincal Wu<sup>1</sup>, Shixun Lin<sup>1</sup>, Yonghai Chen<sup>1</sup> and Jinfang Zheng<sup>1\*</sup> 

## Abstract

**Background:** The aim of this study was to construct a model based on the prognostic features associated with epithelial–mesenchymal transition (EMT) to explore the various mechanisms and therapeutic strategies available for the treatment of metastasis and invasion by hepatocellular carcinoma (HCC) cells.

**Methods:** EMT-associated genes were identified, and their molecular subtypes were determined by consistent clustering analysis. The differentially expressed genes (DEGs) among the molecular subtypes were ascertained using the limma package and they were subjected to functional enrichment analysis. The immune cell scores of the molecular subtypes were evaluated using ESTIMATE, MCPcounter, and GSCA packages of R. A multi-gene prognostic model was constructed using lasso regression, and the immunotherapeutic effects of the model were analyzed using the Imvigor210 cohort. In addition, immunohistochemical analysis was performed on a cohort of HCC tissue to validate gene expression.

**Results:** Based on the 59 EMT-associated genes identified, the 365—liver hepatocellular carcinoma (LIHC) samples were divided into two subtypes, C1 and C2. The C1 subtype mostly showed poor prognosis, had higher immune scores compared to the C2 subtype, and showed greater correlation with pathways of tumor progression. A four-gene signature construct was fabricated based on the 1130 DEGs among the subtypes. The construct was highly robust and showed stable predictive efficacy when validated using datasets from different platforms (HCCDB18 and GSE14520). Additionally, compared to currently existing models, our model demonstrated better performance. The results of the immunotherapy cohort showed that patients in the low-risk group have a better immune response, leading to a better patient's prognosis. Immunohistochemical analysis revealed that the expression levels of the FTCD, PON1, and TMEM45A were significantly over-expressed in 41 normal samples compared to HCC samples, while that of the G6PD was significantly over-expressed in cancerous tissues.

**Conclusions:** The four-gene signature construct fabricated based on the EMT-associated genes provides valuable information to further study the pathogenesis and clinical management of HCC.

**Keywords:** EMT, HCC, Prognosis, G6PD

## Background

Liver cancer is the sixth most common type of cancer in the world and the third leading cause of cancer-related deaths worldwide, with high morbidity and mortality as well as an extremely poor prognosis [1]. Hepatocellular carcinoma (HCC) is the most common type of liver cancer, accounting for 85–90% of all primary liver cancers

\*Correspondence: zhengjf2000@hainmc.edu.cn

<sup>1</sup> Department of Hepatobiliary and Pancreatic Surgery, Hainan General Hospital, Hainan Affiliated Hospital of Hainan Medical University, Haikou, Hainan, China

Full list of author information is available at the end of the article



© The Author(s) 2021. **Open Access** This article is licensed under a Creative Commons Attribution 4.0 International License, which permits use, sharing, adaptation, distribution and reproduction in any medium or format, as long as you give appropriate credit to the original author(s) and the source, provide a link to the Creative Commons licence, and indicate if changes were made. The images or other third party material in this article are included in the article's Creative Commons licence, unless indicated otherwise in a credit line to the material. If material is not included in the article's Creative Commons licence and your intended use is not permitted by statutory regulation or exceeds the permitted use, you will need to obtain permission directly from the copyright holder. To view a copy of this licence, visit <http://creativecommons.org/licenses/by/4.0/>. The Creative Commons Public Domain Dedication waiver (<http://creativecommons.org/publicdomain/zero/1.0/>) applies to the data made available in this article, unless otherwise stated in a credit line to the data.

and causing 700,000 deaths worldwide each year; it is more prevalent and fatal in developing countries [2–4]. Until recently, Sorafenib, a kinase inhibitor drug, was the only systemic treatment option available for patients with advanced HCC. In 2020, atezolizumab and bevacizumab combination therapy turned into a new frontline standard of care for unresectable or metastatic HCC [5]. Despite advancement in treatment strategies in recent decades, the overall 5-year survival rate of patients with HCC is currently less than 12%. This is primarily due to the high recurrence rate and the intra- or extra-hepatic metastases. Most patients with HCC are diagnosed at the advanced stage and therefore, experience limited clinical benefit from treatment [6–9]. Since HCC has a rather poor prognosis and is highly resistant to most anticancer therapies, efforts have been made to unravel the complex molecular mechanisms underlying hepatocarcinogenesis and progression, including epithelial mesenchymal transition (EMT), tumor-stromal interactions, tumor microenvironment, tumor stem cells, and evasion of senescence [10]. A better understanding of these mechanisms can enable the development of new and more effective therapeutic and prognostic strategies, which is the need of the hour.

EMT is an important biological process in embryonic development, cell differentiation and reprogramming, and cancer progression [11, 12]. A growing body of evidence suggests that EMT confers tumor stem cell-like features, which results in treatment resistance and tumor recurrence [13]. Therefore, EMT is considered as one of the primary mechanisms determining cancer cell invasion and metastasis [14]. Much evidence suggests that EMT is associated with the invasion and progression of various malignancies, including HCC [15, 16]. EMT in HCC cells, similar to other tumors, appears to be driven by the aberrant activation of the Wnt/ $\beta$ -catenin signaling pathway [17–20], which increases hypoxia-induced EMT in HCC [21]. Mounting evidence suggests that EMT aids in cell proliferation, invasion, and metastasis during HCC progression, and contributes to chemotherapy resistance, thereby leading to poor patient prognosis [22–24]. In addition, EMT has also been found to positively correlate with resistance to sorafenib, cis-platin, and Adriamycin [25–27]. However, a previous study has revealed that sorafenib inhibits the migration of HCC cells by inhibiting EMT, which is one of the potential mechanisms responsible for the antitumor effect of sorafenib in HCC [28]. Although the mechanisms underlying EMT in HCC have been extensively studied, the prognostic value and the biological role of EMT-associated genes have not been elucidated. Therefore, studying the molecular subtypes of HCC with respect to EMT, and

evaluating their prognostic relevance, is of great importance to identify therapeutic targets and improve the prognosis of HCC patients.

In this study, we identified certain EMT-associated genes and constructed molecular subtypes of liver hepatocellular carcinoma (LIHC) models based on EMT. Subsequently, we evaluated the relationship between the molecular subtypes, and their prognostic and clinical features. A four-gene signature (*PON1*, *FTCD*, *G6PD*, and *TMEM45A*) prognostic risk model was constructed using the DEGs identified among the LIHC molecular subtypes and validated using the HCCDB and GEO gene expression datasets. On validation, we found that the constructed four-gene prognostic marker showed good performance, therefore proving useful for the prognostic classification of HCC patients and identification of new therapeutic targets for HCC.

## Materials and methods

### Data source and pre-processing

The expression data and clinical follow-up information coming from LIHC patient tissues were downloaded using TCGA, and the data were processed through the following steps: (1) Samples without clinical follow-up information were removed. (2) Ensemble was converted to Gene Symbol. (3) The middle value was taken in the presence of multiple Gene Symbol expressions.

The GSE14520 microarray dataset was downloaded from Gene Expression Omnibus (GEO), and the GEO dataset was processed with the following steps: (1) Samples without clinical follow-up information were removed. (2) Probes were converted to Gene Symbols. (3) Removal of probe corresponding to multiple genes. (4) The middle value was taken in the presence of multiple Gene Symbol expressions.

The HCCDB18 data were downloaded from the HCCDB18 database (<http://lifeome.net/database/hccdb/home.html>), and the RNA-Seq data were processed in the following steps: (1) Samples without clinical follow-up information were removed. (2) Samples without expression profile data were removed.

The genes of EMT-associated pathways (HALLMARK\_EPITHELIAL\_MESENCHYMAL\_TRANSITION) were downloaded from Molecular Signature Database v7.0 (MSigDB), and a total of 200 EMT-associated genes were collated and gathered.

After preprocessing three datasets, a total of 365 samples for TCGA-LIHC, 203 samples for HCCDB18, and 221 samples for GSE14520 were attained. The clinical statistical information of the samples is shown in Table 1.

**Table 1** Cohorts information

Clinical features	TCGA-LIHC	HCCDB18	GSE14520
OS			
0	235	168	136
1	130	35	85
T stage			
T1	180		
T2	91		
T3	78		
T4	13		
TX	3		
N stage			
N0	248		
N1	4		
NX	113		
M stage			
M0	263		
M1	3		
MX	99		
Stage			
I	170		
II	84		
III	83		
IV	4		
X	24		
Grade			
G1	55		
G2	175		
G3	118		
G4	12		
GX	5		
Gender			
Male	246		
Female	119		
Age			
≤ 60	173		
> 60	192		
Recurrence			
Yes	198		
No	167		

**Identification of molecular subtypes using the ConsensusClusterPlus algorithm**

The TCGA expression profile data were first filtered by the process of removing genes having expressions less than 1, which accounted for less than 50% of all samples, and a univariate COX analysis was performed to filter out unnecessary genes at a threshold of  $P < 0.05$ . EMT genes associated with prognosis were obtained, followed by the application of consistent clustering of

TCGA samples using ConsensusClusterPlus (V1.48.0; parameters: reps = 100, pItem = 0.8, pFeature = 1, distance = “spearman”).

D2 and Euclidean distance were used as clustering algorithms and distance metrics respectively to obtain molecular subtypes. DEGs between molecular subtypes were calculated using the limma package and subjected to functional enrichment analysis. GSEA was used in the LIHC dataset to analyze the significantly enriched pathways in different groups, where the selected gene set was c2.cp.kegg.v7.0.symbols.gmt that contains the KEGG pathway. The GSEA input file containing the TCGA expression profile data and the molecular subtype were labeled as C1 or C2 group according to the sample labels. The enriched pathways were selected having a threshold of  $p < 0.05$  and  $FDR < 0.25$  as the basis.

**Construction of prognostic risk model based on EMT genes Partitioning of the training and validation sets**

A total of 365 samples in the TCGA dataset were subdivided into training and validation sets. In advance, all samples were randomly grouped 100 times with replacement and group sampling was performed in the ratio of training set: validation set = 1:1 to avoid random assignment bias affecting the stability of subsequent modeling. The most suitable training and validation sets were selected based on the following set conditions: (1) the two groups had to have similar age distribution, gender, follow-up time, and the proportion of patient deaths; (2) there was a similar number of dichotomous samples between the randomly grouped cohorts following gene expression profile clustering. The selection yielded 182 samples in the training set and 183 in the validation set.

The information on both the training and validation set samples of the TCGA data, shown in Table 2, were tested using the chi-square test and showed a validated grouping method having no significant difference between groups ( $p > 0.05$ ).

**Lasso cox regression analysis**

The lasso regression was employed on prognostic genes to reduce the number of genes found in the risk model. Lasso method is a type of shrinkage estimation that obtains a more refined model by constructing a penalty function that allows shrinking of coefficients, setting some coefficients to zero, and retaining the advantage of subset shrinkage. This is a biased estimate that deals with data multicollinearity that achieves variable selection, parameter estimation, and problem-solving capabilities for multicollinearity in regression analysis. The trajectory of each independent variable was analyzed by performing lasso cox regression using the R package glmnet. Subsequently, an optimal model was constructed using fivefold

**Table 2** Sample information of TCGA training set and validation set

Clinical features	TCGA-LIHC train	TCGA-LIHC test	P
OS			
0	116	119	0.8822
1	66	64	
T stage			
T1	94	86	0.3129
T2	37	54	
T3	41	37	
T4	8	5	
TX	2	1	
N stage			
N0	123	125	0.5998
N1	3	1	
NX	56	57	
M stage			
M0	132	131	0.1966
M1	3	0	
MX	47	52	
Stage			
I	90	80	0.3149
II	34	50	
III	43	40	
IV	3	1	
X	12	12	
Grade			
G1	29	26	0.9548
G2	88	87	
G3	56	62	
G4	6	6	
GX	3	2	
Gender			
Male	119	127	0.48
Female	63	56	
Age			
≤ 60	87	86	0.9604
> 60	95	97	

cross-validation to analyze the confidence intervals under each lambda and to find the number of targeted genes.

### Immunohistochemistry

To verify the expression of the candidate four genes, tissue microarrays (TMA) comprised of 41 HCC tissues and 41 normal samples were obtained from Shanghai Outdo Biotech Co., Ltd. (Shanghai, China). The studies were conducted in accordance with the International Ethical Guidelines for Biomedical Research Involving Human Subjects (CIOMS), and the research protocols

were approved by the Ethics Committee of Hainan General Hospital, Hainan Affiliated Hospital of Hainan Medical University.

The TMA slides were dried overnight at 37 °C, dewaxed in xylene, and dehydrated in a gradient ethanol series. Antigen's retrieval was performed by heating the tissue sections in a microwave oven inside a vessel filled with EDTA antigen retrieval buffer (pH 9.0). Subsequently, the tissue sections were immersed in 3% hydrogen peroxide for 25 min to block the activity of endogenous peroxides. Next, the TMA tissues were coated with 3% bovine serum albumin (BSA) and sealed at room temperature for 30 min to reduce non-specific staining. Then, the TMA slides were incubated with anti-TMEM45A (1:500 dilution; Sigma, HPA062101), anti-PON1 (1:100 dilution; Abcam, ab92466), anti-FTCD (1:250 dilution; Abcam, ab129005) and anti-G6PD (1:2000 dilution; Abcam, ab210702) overnight at 4 °C.

The tissues were rinsed with 0.01 mol/L phosphate buffer saline (PBS; pH=7.4) for 5 min each. The tissues were incubated at room temperature for 50 min with horseradish peroxidase (HRP)-labeled goat anti-rabbit secondary antibody (1:200 dilution, ServiceBio, GB23303). Then, the tissues were washed in PBS and stained with 3,3-diaminobenzidine (DAB). Finally, the TMA sections were counterstained with Mayer's hematoxylin, dehydrated, and fixed. To evaluate IHC staining, semi-quantitative scoring criteria were used.

The stained sections were scored by three pathologists who were blinded to the patients' clinical characteristics. The scoring system was based on the proportion of positively stained cells in all tissues and the staining intensity of these positively stained cells. The staining intensity was classified as follows: 0 (negative), 1 (weak), 2 (moderate), or 3 (strong). The staining ratio of positive cells was classified as follows: 0 (<5%), 1 (5–25%), 2 (26–50%), 3 (51–75%), or 4 (>75%). According to the staining intensity and the proportion of positively stained cells, the tissues were graded as follows: 0–1 grade, negative (–); >1–4, weakly positive (+); >4–8, moderately positive (++) and >8–12, strongly positive (+++).

### Results

Identification of molecular subtypes using non-negative matrix factorization (NMF) algorithm

The expression of 200 EMT genes was first extracted from the TCGA expression profile data, followed by univariate cox analysis by coxph function in R. Fifty-nine genes (Additional file 1: Table S1) associated with LIHC prognosis ( $p < 0.05$ ) were obtained, and the LIHC samples were clustered by non-negative matrix factorization algorithm (NMF). An optimal clustering of  $k=2$  was determined based on cophenetic, a residual sum of squares,

and other metrics, thus obtaining two molecular subtypes (C1, C2) (Fig. 1A–C).

Further analysis on the prognostic relationship between subtypes revealed a significant difference between C1 and C2 groups in terms of overall survival (OS) time and disease-specific survival (DSS) time (Fig. 1D, E, log-rank  $p < 0.01$ ). It was also found that the C1 subtype carried a poorer prognosis.

**Comparison and analysis of immune and matrix scores between molecular subtypes**

The different clinical features in two molecular subtypes were compared, the results revealed that (1) survival rates were significantly different amongst the two subtypes and the C1 group showed a poorer prognosis (Fig. 2A); (2) the proportion of T-stage was significantly different between the two subtypes, and a higher proportion of T2, T3, and T4 in the C1 group carried a poor prognosis (Fig. 2B); (3) the proportion of Stage was significantly different

between the two subtypes, with a higher proportion of Stage II and III in the C1 group with poor prognosis (Fig. 2C); (4) the proportion of Grade was significantly different between the two subtypes, with a higher proportion of G3 in the C1 group having poor prognosis (Fig. 2D).

The six types of immune infiltration identified in human tumors are as follows: C1 (wound healing), C2 (INF-r dominant), C3 (inflammation), C4 (lymphocyte depletion), C5 (immunologically silent,) and C6 (TGF-beta dominant) [29]. Utilizing this subtyping outcome, KM curves were plotted and found that the immune subtype C1 had the worst prognosis (Fig. 2G, H). A comparison was made between this subtyping method and the study’s subtyping sample (Fig. 2E, F) and an analysis of the distribution of this subtyping against the study’s EMT molecular subtypes indicated a consistent tendency that immune subtype C1 was more distributed in the molecular subtype C1.

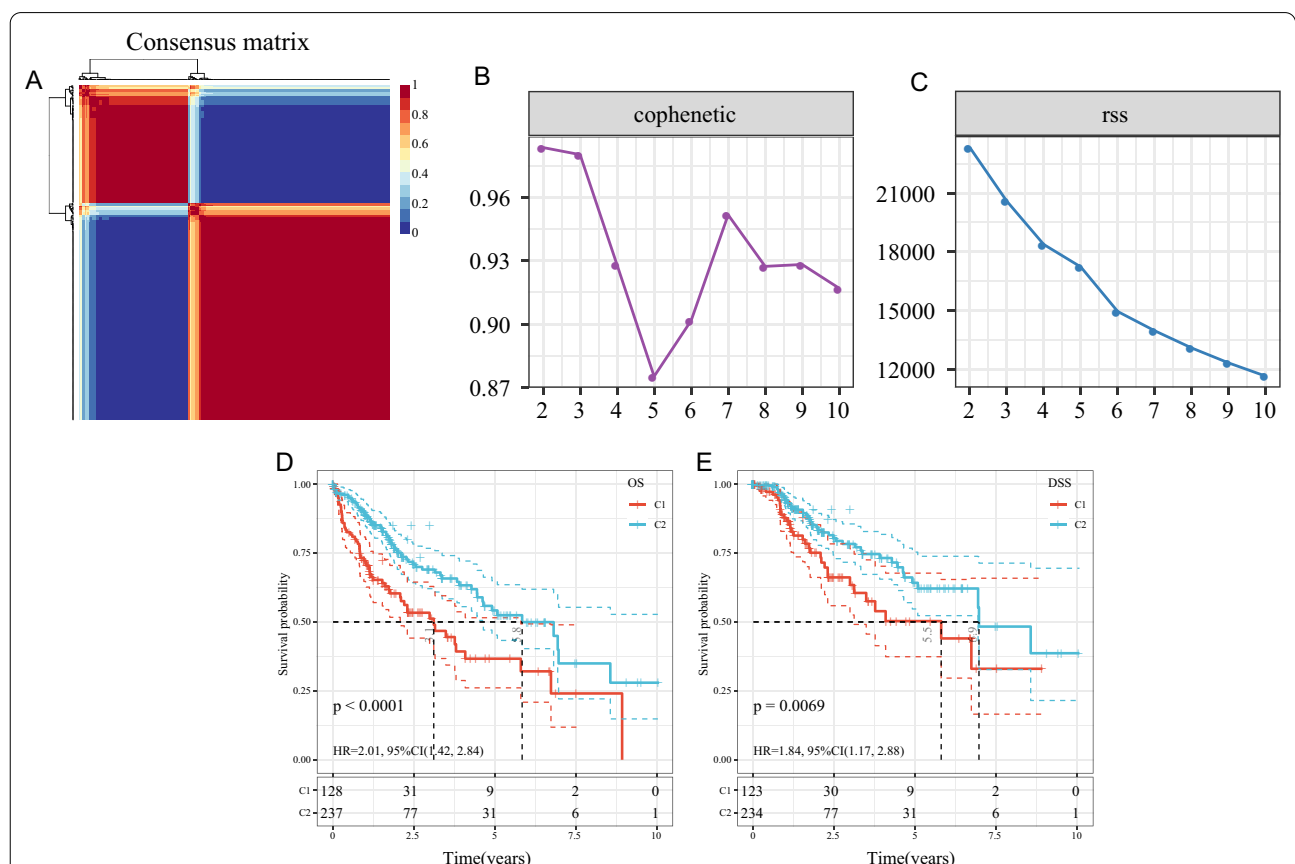
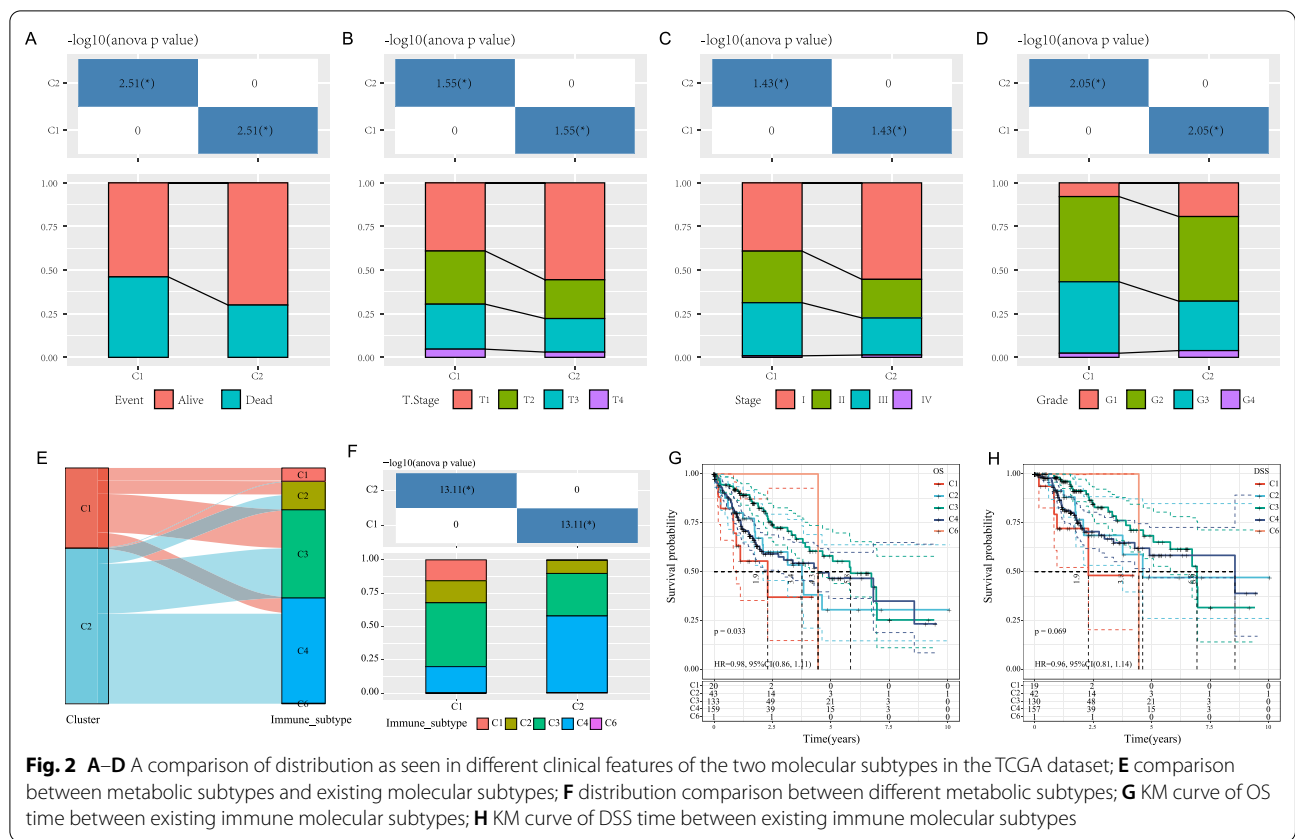


**Fig. 1** **A** Consensus map of NMF clustering; **B** cophenetic distribution having rank = 2–10, where cophenetic correlation is obtained from the consistency matrix proposed by Brunet et al. that is reflective of the stability of the cluster obtained from NMF. The value is between 0 and 1, where a larger value signified a more stable cluster; **C** the rss distribution with rank = 2–10. Rss is the residual sum of squares and shows clustering performance of a model, where a smaller value yielded a better clustering effect of the model in contrast to the theoretical concept that the smallest value is attained when each sample is clustered into one class; **D** overall survival (OS) time prognosis survival curve of LIHC molecular subtypes; **E** DSS time prognosis survival curve of LIHC molecular subtypes



### Comparison of immune scores between molecular subtypes

To identify the relationship of immune scores between molecular subtypes in the TCGA dataset, the R software package ESTIMATE was used to evaluate three immune scores of StromalScore, ImmuneScore, and ESTIMATEScore. Ten and twenty-two immune cells scores were also evaluated using MCPcounter and CIBERSOTR, respectively.

Comparing the differences of immune scores in molecular subtypes (Fig. 3A–C) elucidated that the immune scores of C1 subtypes were generally higher than C2 subtypes as seen in the three software. Heat maps of the immune score also visually demonstrated the differences in immune scores between subtypes (Fig. 3D).

### Identification of DEGs between subtypes and functional analysis of pathways

DEGs between C1 and C2 molecular subtypes were calculated using the limma package, with a total of 1130 DEGs filtered according to the threshold  $FDR < 0.01$  and  $|\log_2FC| > 1$ , of which 931 were up-regulated genes and 199 were down-regulated genes. An up-regulated expression pattern between C1 and C2 was the predominant form (Fig. 4A). The DEGs are shown in Additional file 2: Table S2 and the 100 genes with the largest up- and down-regulation were selected and plotted in the heat map (Fig. 4B).

The KEGG pathway analysis and GO functional enrichment analysis were performed on 931 up-regulated differential genes of LIHC subtypes using the Gplot R package, in which 1001 annotated genes showed significant differences in Biological Process (BP) (Fig. 4C,  $FDR < 0.05$ ).

(See figure on next page.)

**Fig. 3** Comparison of immune scores as seen in the three-immune software between molecular subtypes of TCGA dataset. **A** Comparison of CIBERSOTR immune scores between molecular subtypes of TCGA dataset; **B** comparison of MCPcounter immune scores between molecular subtypes of TCGA dataset; **C** comparison of ESTIMATE immune scores between molecular subtypes of TCGA dataset; **D** comparison of three immune software immune scores between molecular subtypes of TCGA dataset

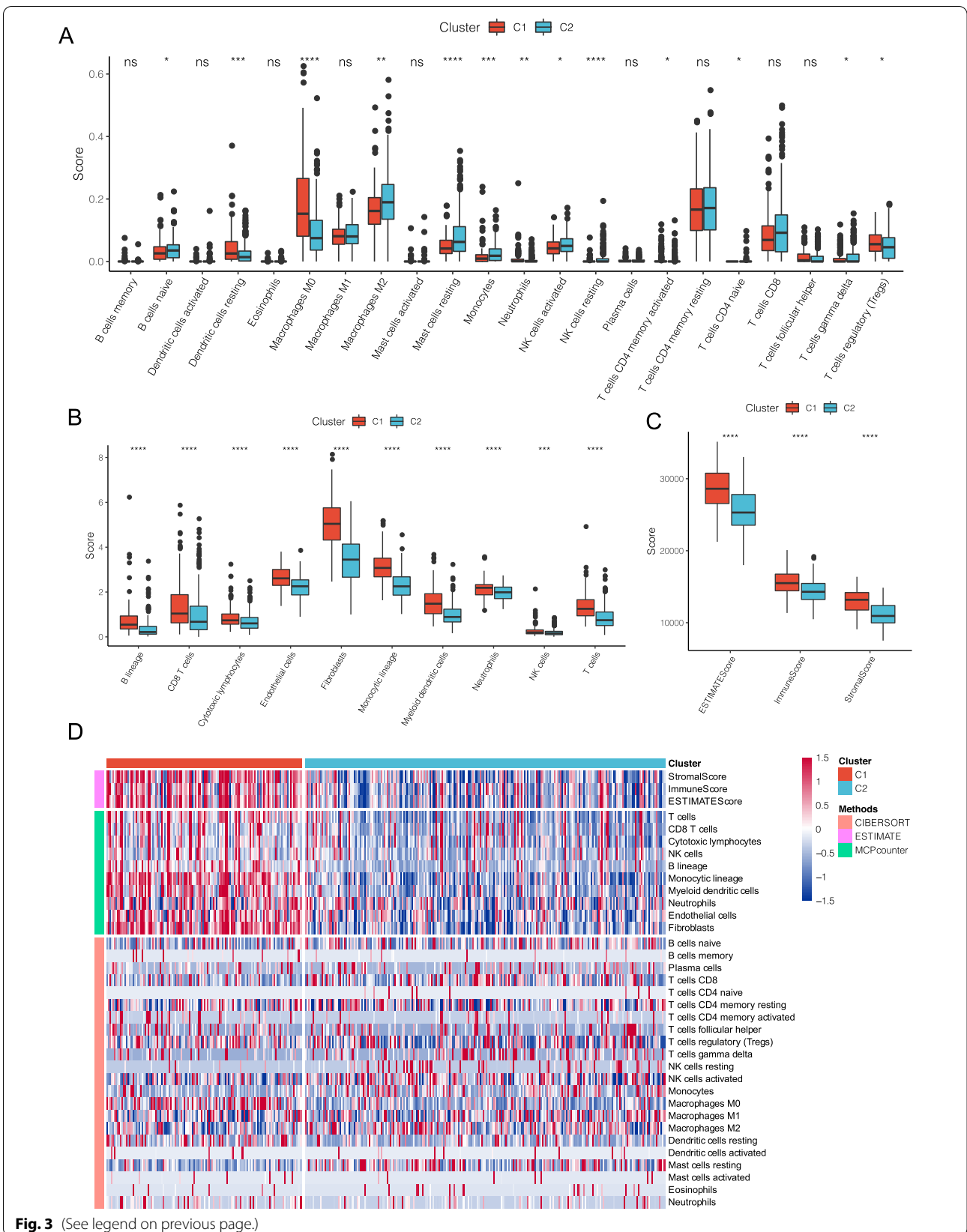
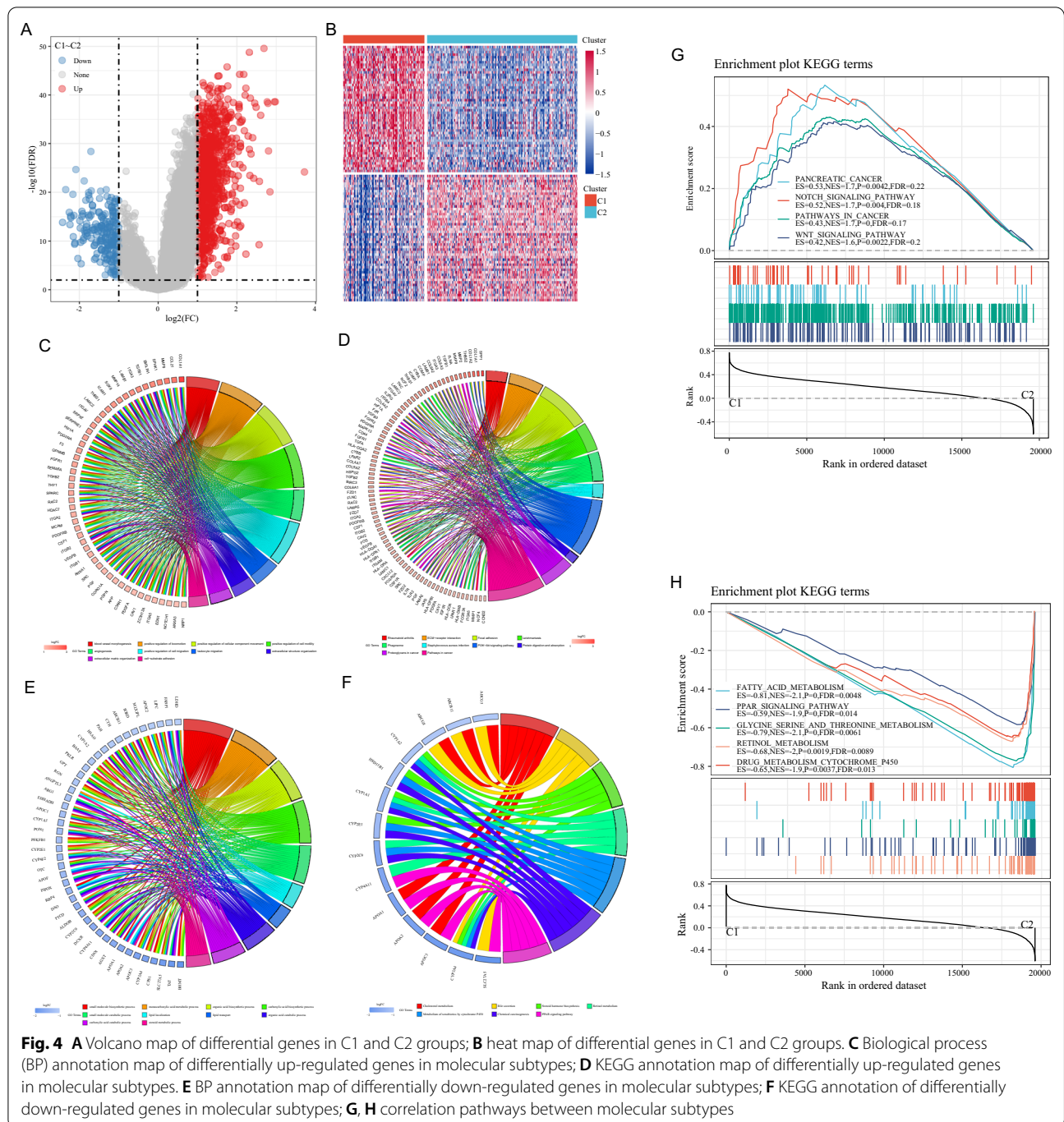


**Fig. 3** (See legend on previous page.)



As to the differential genes of LIHC, KEGG pathway enrichment was performed and genes were significantly enriched in: ECM-receptor interaction, Proteoglycans in cancer, Rap1 signaling pathway, PI3K-Akt signaling pathway, Pathways in cancer, and other tumor-related pathways (Fig. 4D). The same approach was used to perform both pathway analysis and functional enrichment analysis for 199 down-regulated differential genes.

The down-regulated genes were also found to be significantly enriched in: retinol metabolism, glycine, serine, and threonine metabolism, metabolism of xenobiotics by cytochrome P450, PPAR signaling pathway, and other metabolism-related pathways (Fig. 4E, F). Further employment of GSEA revealed that PATHWAYS\_IN\_CANCER, WNT\_SIGNALING\_PATHWAY, and NOTCH\_SIGNALING\_PATHWAY and



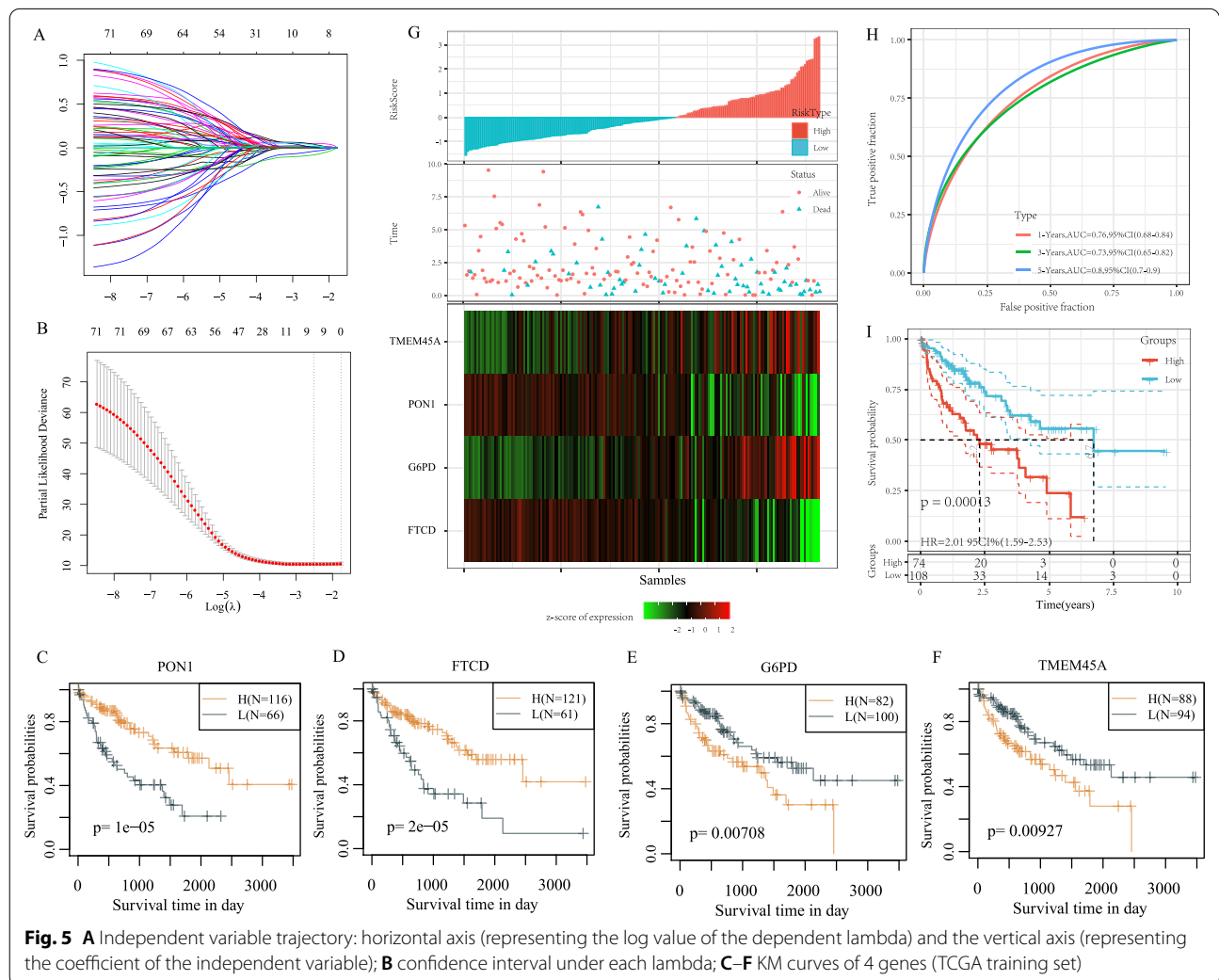
other tumor-related pathways were enriched in the C1 subtype group (Fig. 4G), thus showing a clear relationship between C1 subtype and tumors; in contrast, metabolism-related pathways such as: FATTY\_ACID\_METABOLISM, PPAR\_SIGNALING\_PATHWAY, and DRUG\_METABOLISM\_CYTOCHROME\_P450 were more enriched in the C2 subtype group (Fig. 4H) depicting a close association between C2 subtype and metabolism.

**Construction of a prognostic risk model**

A total of 182 samples were obtained from the training set while 183 samples were derived from the validation set (Table 2). The data in the training set (a total of 1130 differential genes of C1 and C2 molecular subtypes) was subjected to the univariate Cox proportional risk regression model and the survival data used the R package surv coxph function, where  $p < 0.01$  was selected as the threshold for filtering and resulted to a total of 71 prognostic

genes (Additional file 3: Table S3). However, these genes are not conducive to clinical testing and still need further reduction using the lasso regression to maintain a high accuracy rate. The R package glmnet was used for lasso cox regression analysis, where the independent variable trajectories were analyzed (Fig. 5A), and the results showed that as lambda gradually increases, the number of independent variable coefficients also gradually increases. Fivefold cross-validation was done to analyze the confidence intervals under each lambda (Fig. 5B) and indicated that the model was optimal when  $\lambda = 0.08091131$ , therefore 9 genes at  $\lambda = 0.08091131$  were selected as the target genes for the next step.

The Akaike Information Criterion (AIC), a stepwise regression, was utilized to take into account the statistical fit of both models and parameters. The AIC method in the MASS package first started off with a complex model that later removed one variable to reduce the AIC



thus resulting in a better model having fewer parameters. Using this algorithm, the final 9 genes were reduced to 4 genes, namely: PON1, FTCD, G6PD, and TMEM45A, and the prognostic KM curves for the 4 genes (Fig. 5C–F) can significantly separate the TCGA training set samples ( $p < 0.05$ ). The final 4-gene signature formula is as follows: RiskScore =  $-0.125 * PON1 - 0.144FTCD + 0.133 * G6PD + 0.134 * TMEM45A$ .

The calculation of RiskScore for each sample was according to the expression levels per sample and the higher the RiskScore correlated with a worse prognosis (Fig. 5G). The R package time ROC performed an analysis for the prognostic classification of RiskScore at 1 year, 3 years, and 5 years, which showed the model with a high AUC above 0.7 (Fig. 5H). Finally, samples with a RiskScore greater than zero and less than zero were classified as high-risk group and low-risk group respectively. A plotted KM curve classified 74 samples as a high-risk group and 108 samples as a low-risk group (Fig. 5I).

### Validation of the risk model

To determine the robustness of the model, a validation set of the TCGA applied the same model and the same coefficients as the training set. The RiskScore distribution of the TCGA validation set (Fig. 6A), showed that LIHC samples with high RiskScores correlating with worse prognosis were significantly smaller than those with low RiskScores. In addition, prognostic prediction efficiency at 1 year, 3 years, and 5 years was analyzed using R package timeROC (Fig. 6B). The plotting of KM curves showed that 77 samples were classified as a high-risk group while 106 samples were categorized as a low-risk group (Fig. 6C,  $p < 0.01$ ).

The distribution of RiskScore for the full TCGA dataset (Fig. 7A) suggested that high RiskScore samples have a worse prognosis and the prognostic prediction efficiency of RiskScore at 1 year, 3 years, and 5 years was analyzed using the R software package timeROC (Fig. 7B). The plotted KM curves showed that 152 samples were

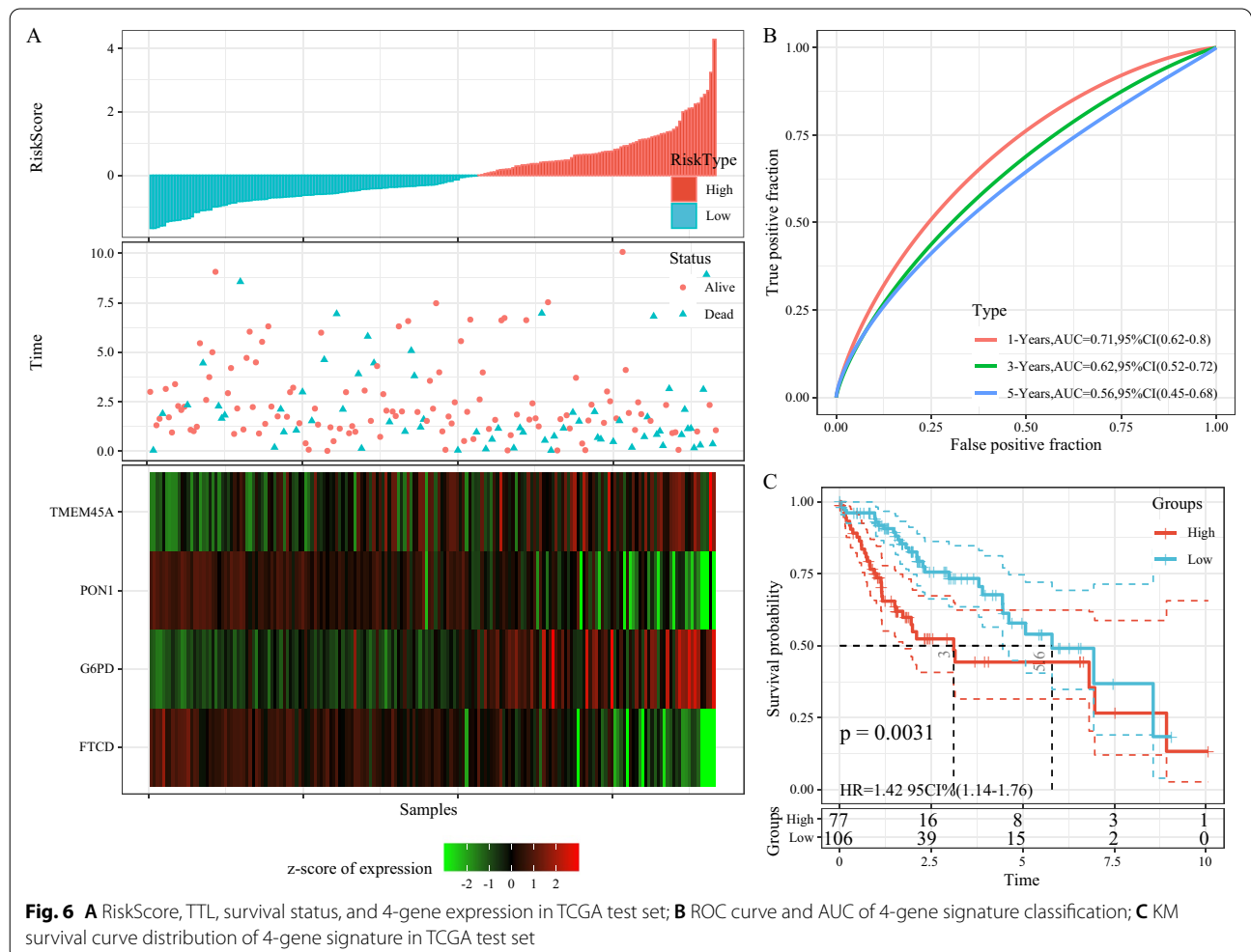
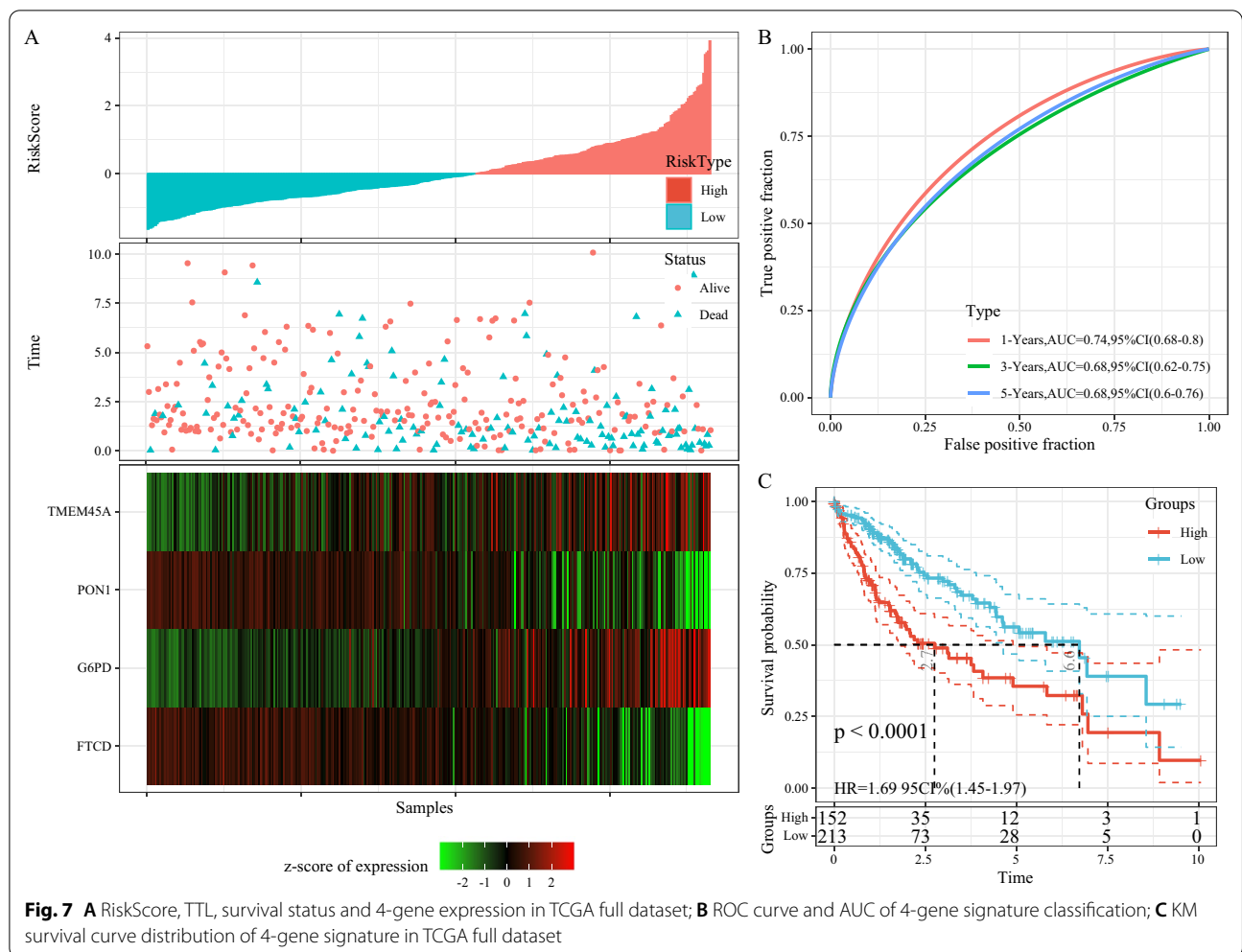


**Fig. 6** **A** RiskScore, TTL, survival status, and 4-gene expression in TCGA test set; **B** ROC curve and AUC of 4-gene signature classification; **C** KM survival curve distribution of 4-gene signature in TCGA test set



classified as a high-risk group and 213 samples as a low-risk group (Fig. 7C,  $p < 0.001$ ).

**Robustness of 4-gene signature verified by external dataset**

The same model and coefficients as in the training set were used in the external validation sets GSE14520 and HCCDB18. The RiskScore of each sample was calculated separately based on the expression level of each sample followed by the plotting of the RiskScore distribution.

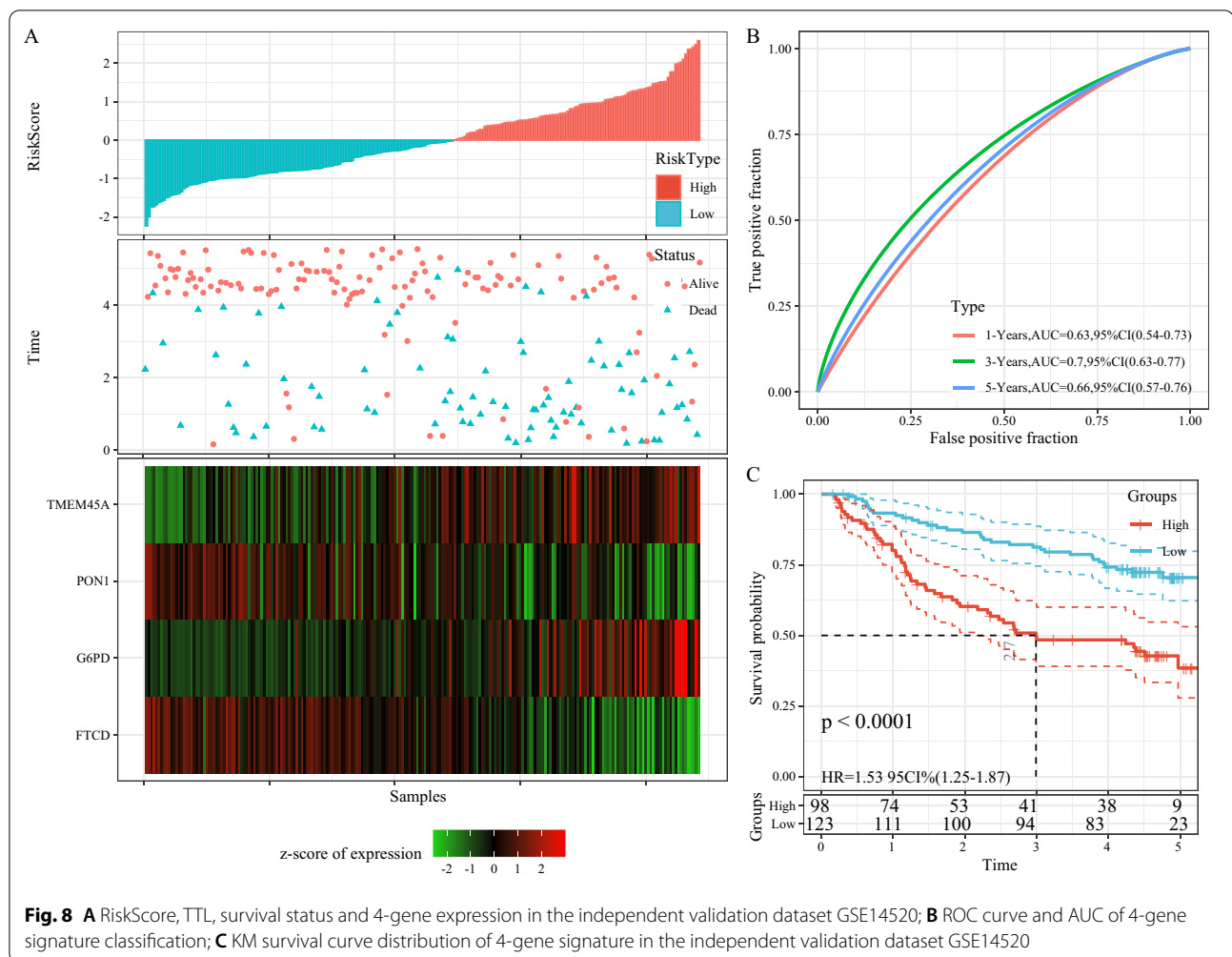
The distribution of RiskScore for independent validation dataset GSE14520 (Fig. 8A) suggested that high RiskScore samples have a worse prognosis and the prognostic prediction efficiency of RiskScore at 1 year, 3 years, and 5 years was analyzed using the R software package timeROC (Fig. 8B). The samples having RiskScore greater than zero and less than zero were classified as high-risk group and low-risk group respectively. The plotted KM curves showed a significant difference, with 98 samples

being classified as a high-risk group and 123 samples as a low-risk group (Fig. 8C,  $p < 0.01$ ).

The distribution of RiskScore for the independent validation dataset HCCDB18 is shown in Fig. 9A. The ROC analysis of RiskScore for prognostic classification was performed using the R software package timeROC. With very few 5-year survival samples from this dataset, only the prognostic prediction of RiskScore at 1 year, 3 years, and 4 years was analyzed (Fig. 9B). The plotted KM curves showed a significant difference, with 91 samples were classified as high-risk group and 112 samples as a low-risk group (Fig. 9C,  $p < 0.01$ ).

**Correlation analysis of risk model having clinical features and pathways**

A 4-gene signature showed it could significantly distinguish the Age, T Stage, N Stage, M Stage, Stage, Grade, and Recurrence groups from the two high-and low-risk groups, respectively (Fig. 10A–I,  $p < 0.05$ ), thus suggestive of the model’s predictive ability. After comparing



the distribution of RiskScore amongst clinical groups, significant differences were found among T Stage, Stage, Grade, and Recurrence groups (Fig. 10J–L,  $p < 0.05$ ), and a more advanced stage correlated with a higher RiskScore. The same is seen with Grade samples, where the higher degree of differentiation correlated with a higher RiskScore and RiskScores of Recurrence samples were higher than the Non-recurrence samples.

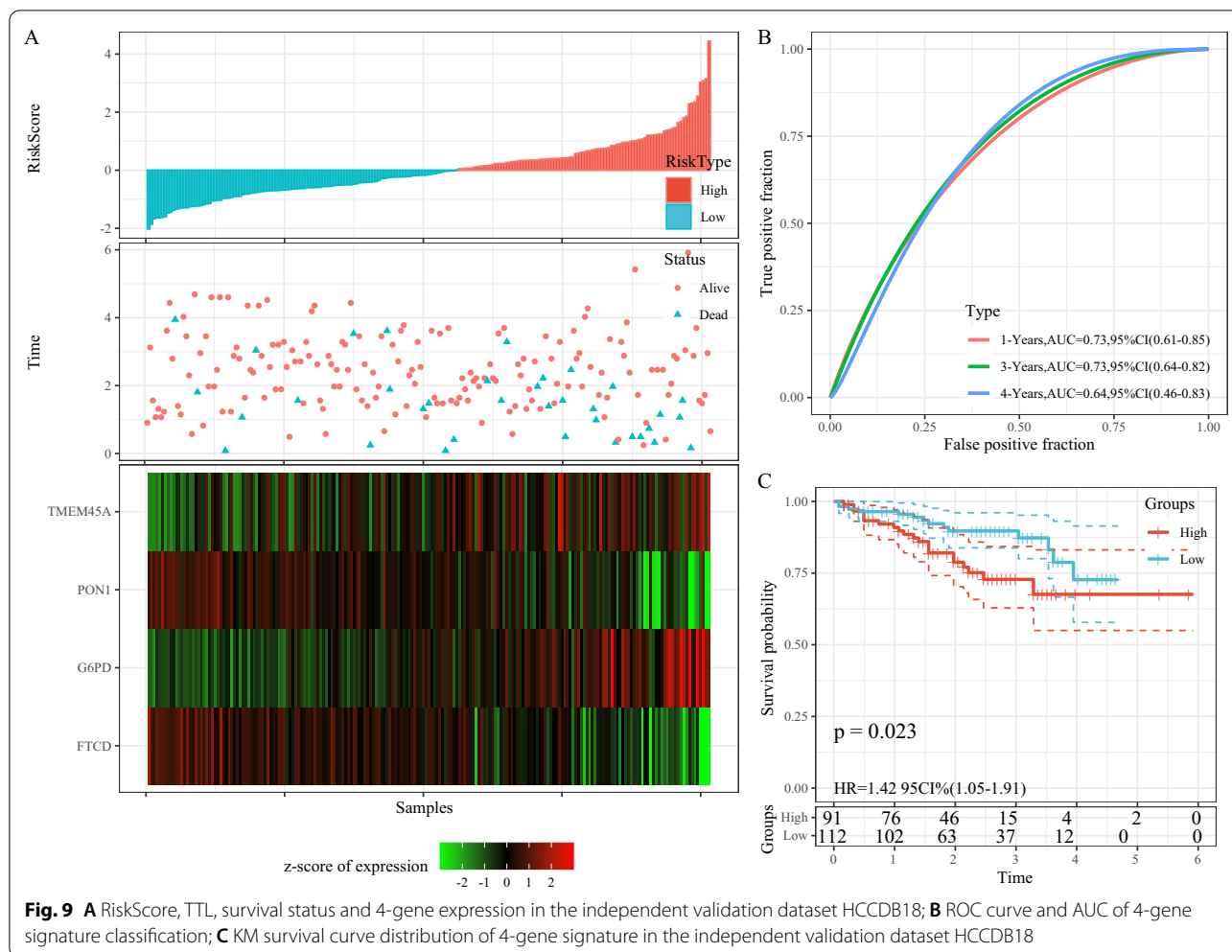
The relationship between RiskScores and biological functions of different samples are observed through corresponding gene expression profiles that were subjected to single-sample GSEA. The ssGSEA scores for each function were calculated for each sample. Then, the correlation between these functions and the RiskScore was further calculated, and a correlation greater than 0.55 was selected in Fig. 10M (4 showing a positive RiskScore correlation and 26 showing a negative RiskScore correlation). The 30 most relevant KEGG Pathways were selected and clustered (Fig. 10N), and those tumor-related pathways: KEGG\_PATHWAYS\_IN\_CANCER and KEGG\_

CELL\_CYCLE increased with increasing RiskScore, and metabolism-related pathways: KEGG\_FATTY\_ACID\_METABOLISM, KEGG\_RETINOL\_METABOLISM, KEGG\_PPAR\_SIGNALING\_PATHWAY, KEGG\_DRUG\_METABOLISM\_CYTOCHROME\_P450 decreased with increasing RiskScore.

The relationship between the immune and matrix scores of the RiskScore was established using the R software package estimate and Pearson correlation coefficient. The calculated values showed that the RiskScore and the StromalScore, ImmuneScore, as well as ESTIMATEScore all showed a significant positive correlation (Fig. 10O–Q,  $P < 0.05$ ).

#### Univariate and multivariate analysis of 4-gene signature

Clinical independence of 4-gene signature in the TCGA dataset was identified using univariate and multivariate COX regression analysis, and the univariate COX regression analysis found that RiskScore was significantly associated with survival and the multivariate COX regression



analysis revealed that RiskScore (HR = 1.86, 95% CI = 1.25–2.76, p = 0.002) remained significantly associated with survival (Fig. 11). The above results indicated that our 4-gene signature model possesses a good clinical predictive performance.

**The comparison of risk model with other models**

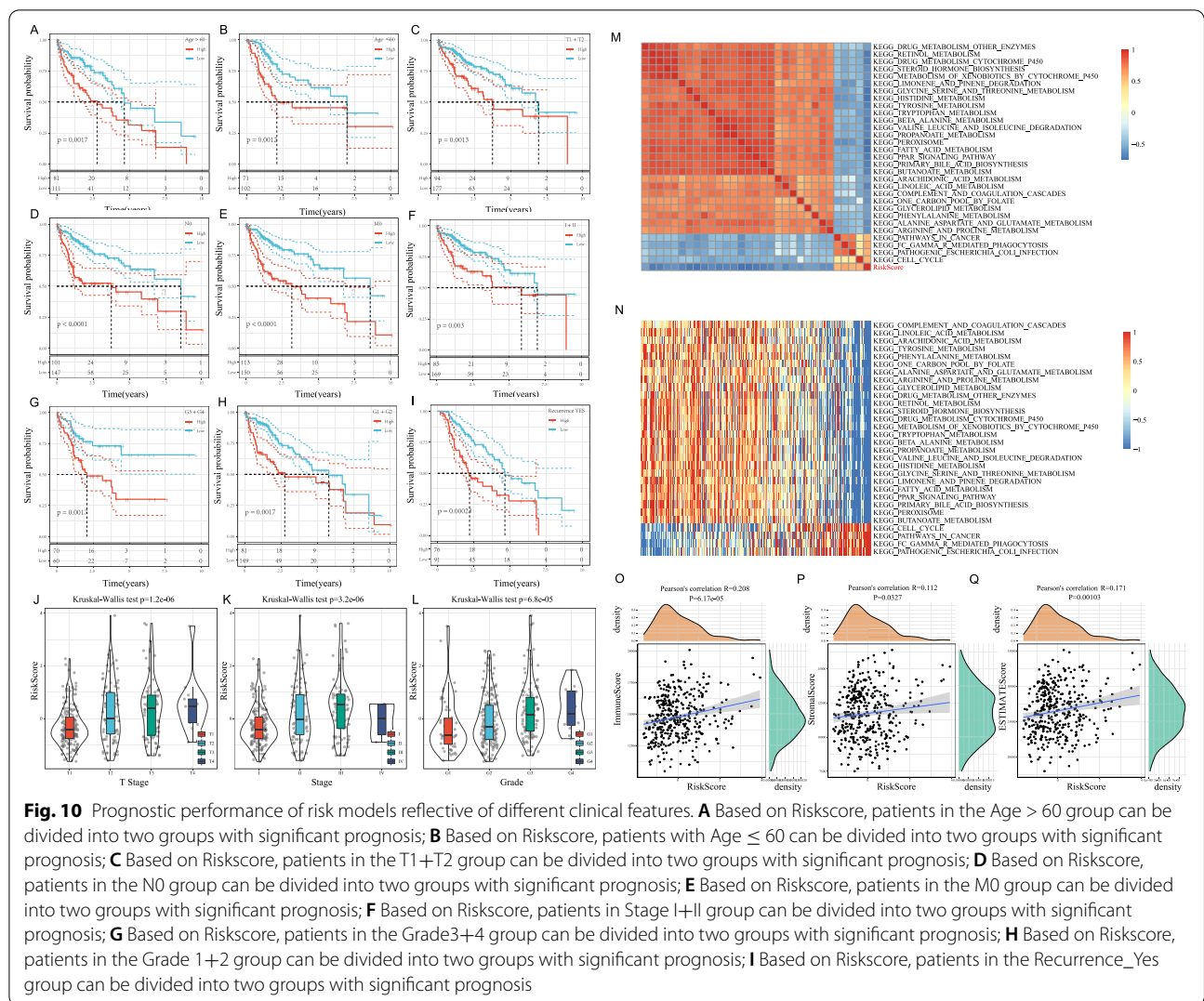
By retrieving the literature, three prognosis-related risk models, namely 4-gene signature (Zheng) [30], 6-gene signature (Ke) [31] and 6-gene signature (Liu) [32] were finally selected for comparison with our 4-gene model. To make models comparable, RiskScores were calculated for each LIHC sample based on the corresponding genes in 3 models. The Riskscore greater than zero were classified as a high-risk group and those with less than zero were classified as a low-risk group. Survival analysis revealed that the prognosis of LIHC differed between the high- and low groups of the three models (Fig. 12B, D, F, log-rank p < 0.05), their 5-year AUC values, however, were lower compared to our model (Fig. 12A, C, E),

highlighting the more reasonable and effective result with a reasonable number of genes.

To compare the predictive performance of these models to the LIHC sample, the concordance index (C-index) of the four model was calculated using the rms package in R. The result showed that our RiskScore model yielded a higher C-index value thus indicating a good predictive performance.

**Prediction of immunotherapy by the risk model**

With the limited effective predictive markers for immunotherapy, there is a critical need to identify novel predictive markers to further advance precision immunotherapy. Imvigor210, an immunotherapy dataset containing transcriptomic data, was retrieved to explore if the 4-genes model could predict the benefit of immunotherapy. This resulted in imvigor210 recording expression data from patients who responded and failed to respond with anti-PD-L1 immunotherapy.



Kaplan–Meier curves showed that higher RiskScore values were associated with poorer survival in mUC patients receiving immunotherapy (Fig. 13A) whereas ROC analysis revealed that the complex model integrating RiskScore, NEO, and TMB had higher predictive performance (Fig. 13B, ROC=0.75). Comparing the RiskScore differences between different groups also showed that patients belonging in the complete response (CR) group had a significantly lower RiskScore than those in the progressive disease (PD) group (Fig. 13C) and that fewer samples were responding to immunotherapy (CR+PR) in the high-risk group than in the low-risk group (18% vs. 26%) (Fig. 13D).

**Immunohistochemical verification of genes in the model**

To verify the expression differences of FTCD, G6PD, PON1 and TMEM45A, protein expressions in 82 cases of HCC and para-cancerous tissues was detected using immunohistochemical assays and reflected higher expressions of FTCD, PON1, and TMEM45A genes in para cancerous tissues (Fig. 14A, C, D) and higher expressions of G6PD genes in cancerous tissues (Fig. 14B). It is important to make mention that the transcript expression of the above genes analyzed in the UALCAN (<http://ualcan.path.uab.edu/>) database was consistent with the data presented in the study (Fig. 14E–H).

**Discussion**

Patients with HCC usually lack clinically significant symptoms in the early stages of the disease. Owing to the high morbidity and mortality associated with the disease,

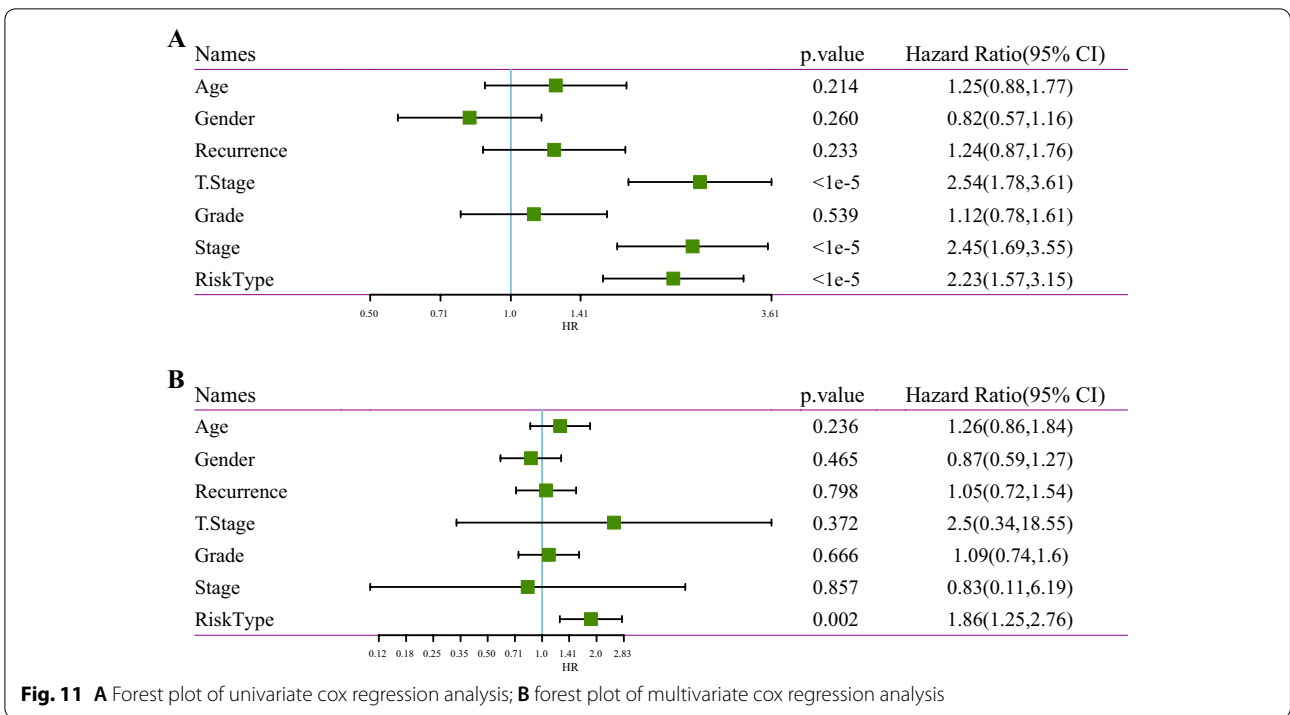
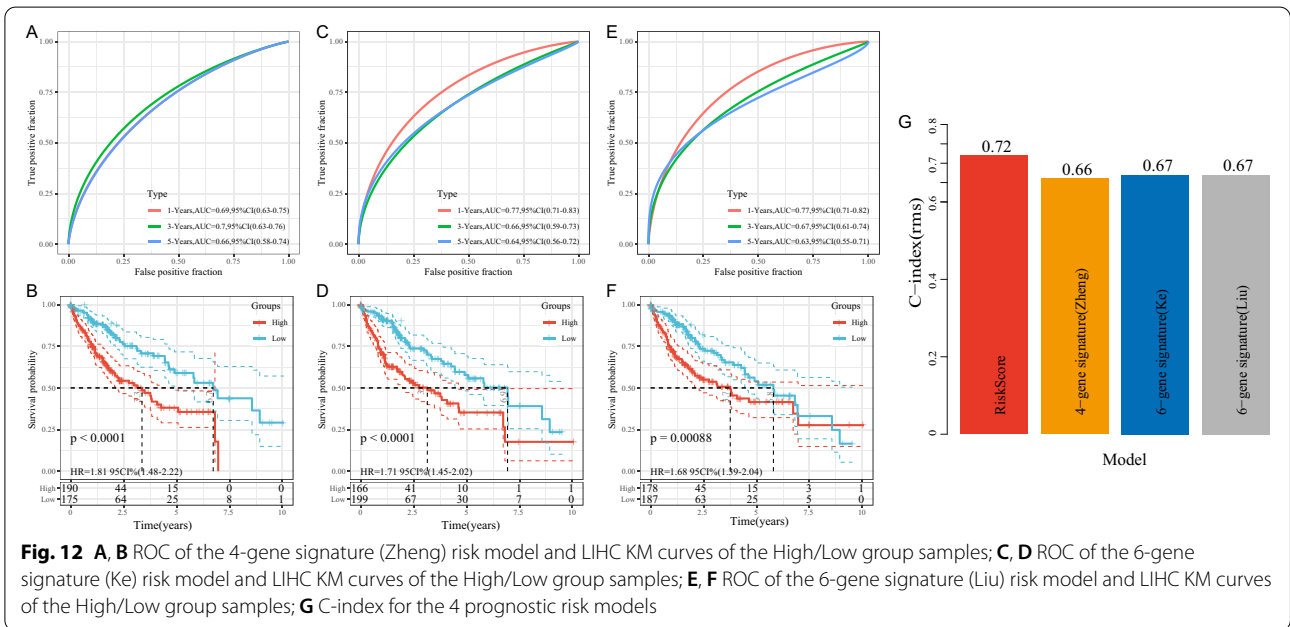


**Fig. 11** **A** Forest plot of univariate cox regression analysis; **B** forest plot of multivariate cox regression analysis



these patients remain a major public health challenge worldwide [33]. Given the enormous heterogeneity of HCC, the identification of new prognostic markers and the construction of more accurate prognostic models are crucial. In this study, we classified 365 LIHC samples from TCGA based on the 59 EMT-associated genes identified, and assigned them to two molecular subtypes

which had different clinical features and prognostic outcomes. In general, the C1 group showed poor prognosis and had a higher proportion of deaths, higher T-stage, higher differentiation degree, more advanced staging, and higher immune scores, compared to the C2 group. Based on this, a prognostic evaluation model was constructed, which not only distinguished the different

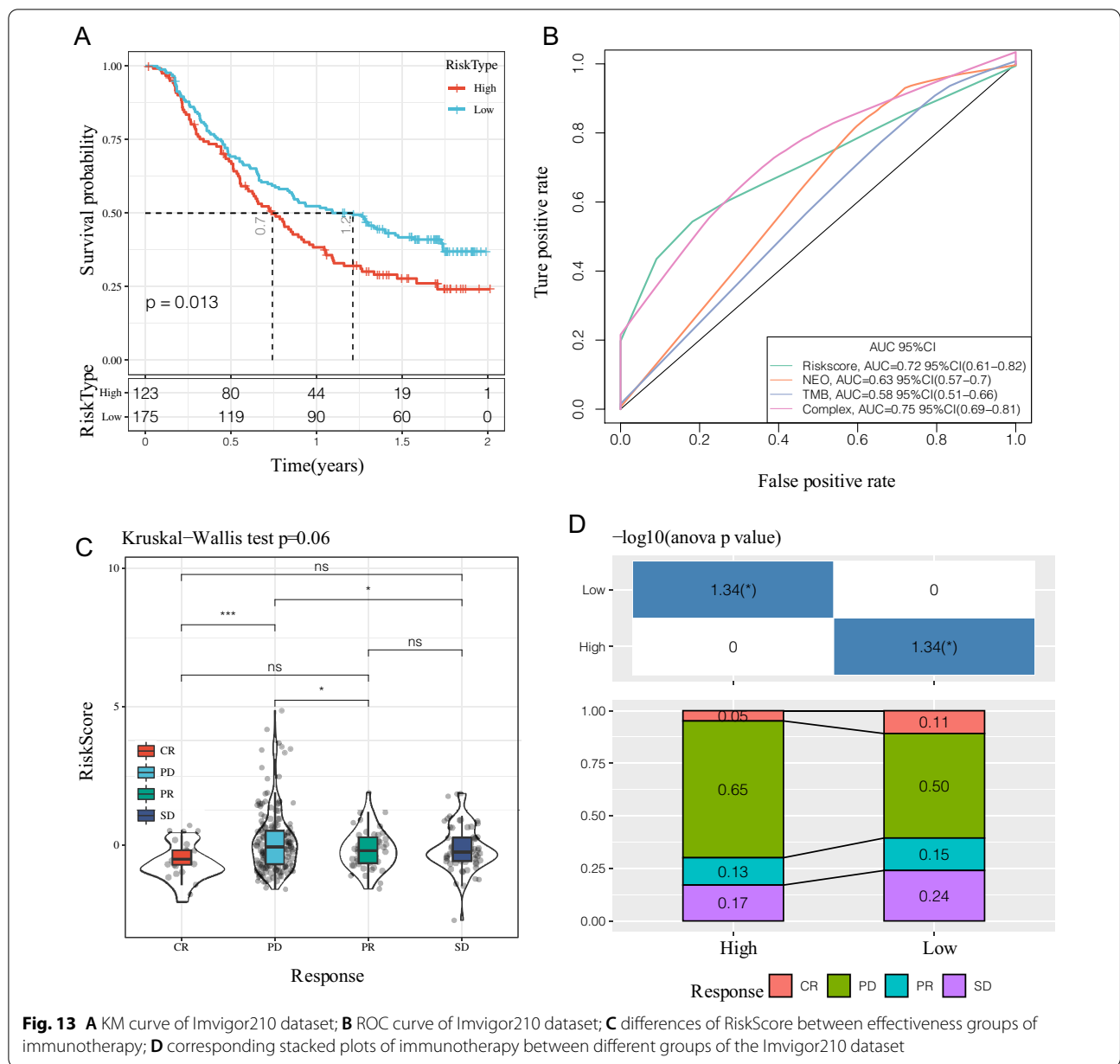


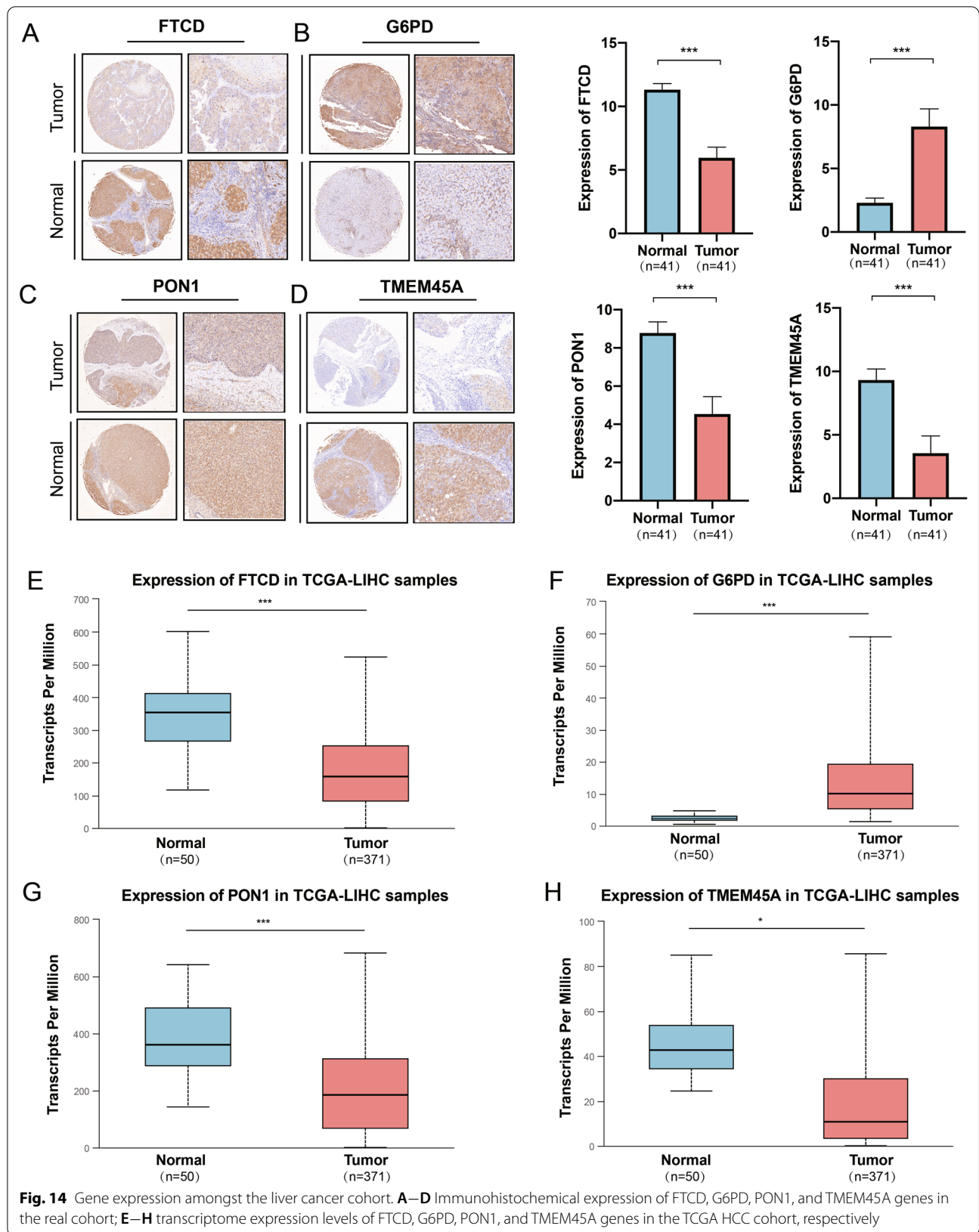
**Fig. 13** **A** KM curve of Imvigor210 dataset; **B** ROC curve of Imvigor210 dataset; **C** differences of RiskScore between effectiveness groups of immunotherapy; **D** corresponding stacked plots of immunotherapy between different groups of the Imvigor210 dataset

molecular subtypes but also better evaluated the prognosis of patients with HCC.

In recent years, increasing number of studies have reported on tumor prognostic models. However, no studies have focused on predicting HCC prognosis based on EMT-associated markers. In this study, we fabricated a novel, highly robust four-gene marker (including *PON1*, *FTCD*, *G6PD*, and *TMEM45A*) for the prediction of HCC prognosis, based on EMT-associated genes, and validated the marker in two other independent cohorts. Paraonase-1 (PON1), a  $\text{Ca}^{2+}$ -dependent high-density lipoprotein

(HDL)-associated endostatin, is the first member of the paraonase (PON) multigene family. It is associated with the antioxidant effect of HDL, possesses athero-protective properties, and is associated with the pathogenesis of many diseases, including cardiovascular disease and cancer [34–36]. A number of studies have shown that PON1 activity is associated with the progression of many cancers [37, 38]. For example, *PON1* gene polymorphism has been associated with breast cancer susceptibility [39], while *PON1* concentration has been positively correlated with the degree of bone destruction in multiple myeloma [40]. Moreover, PON1





activity is elevated in the serum of patients with colorectal cancer and tissues of patients with colon cancer [41]. In addition, since serum PON1 concentration is significantly reduced following radiotherapy, it can be used as an indicator of radiotherapy efficacy [42, 43]. PON1 has also been extensively studied in HCC [44–48]. Currently, serum PON1 is used as a biomarker to assess microvascular infiltration in HCC [49, 50].

Formimidoyl transferase cyclodeaminase (FTCD) catalyzes the degradation of histidine during folate metabolism. In addition, it has also been found associated with the Golgi complex [51]. The *FTCD* gene, a candidate tumor suppressor gene in HCC [52], is significantly downregulated in HCC tumor tissues. Therefore, it serves as a useful diagnostic biomarker for distinguishing early stage HCC from benign tumors [53]. Moreover, most hepatocellular and metastatic cancers are diagnosed by examining the combined expression of arginase 1 + FTCD + MOC 31 [54]. In addition, FTCD has also been found to correlate with drug sensitivity to methotrexate chemotherapy [55].

Glucose-6-phosphate dehydrogenase (G6PD) is the rate-limiting enzyme of the pentose phosphate pathway, and its deficiency results in one of the most commonly inherited enzyme deficiency disorders. Reduced NADPH, which is produced by G6PD, is essential for the maintenance of intracellular redox homeostasis and reductive biosynthesis [56]. G6PD is frequently activated in human malignancies to produce precursors for nucleotide and lipid synthesis. The abnormal activation of G6PD leads to proliferation of a variety of cancer cells [57]. G6PD activity is increased in several cancer types, including esophageal, gastric, colorectal, bladder, breast, and lung cancers [58–60]. Increased expression levels of G6PD mRNA results in poor clinical outcomes in cancer patients, including increased drug resistance, and tumor cell migration or proliferation. Therefore, G6PD has been predicted as a valuable potential target for cancer therapy in the near future [61]. In particular, one study has identified G6PD as an important miR-122 target that regulates glucose metabolism in HCC. In addition, the upregulation of G6PD has been reported to be associated with higher tumor grade, increased tumor recurrence, and poor survival in patients with HCC [62].

TMEM45A is a member of the transmembrane protein (TMEM) family. These proteins are components of various cell membranes including the mitochondrial, endoplasmic reticulum, and Golgi membranes [63]. TMEM45A has been reported to be associated with chemotherapy resistance in human breast cancer and HCC cells under hypoxic conditions. It also affects the proliferation and invasion of human ovarian cancer and glioma cells [64–67]. *TMEM45A* gene knockdown has

been found to be effective in inhibiting multidrug resistance and suppressing EMT by inhibiting the TGF- $\beta$  signaling pathway in human colorectal cancer cells [68]. These studies suggest that TMEM45A may be a potential biomarker. In our study, we found that the four-gene marker construct was involved in a wide range of tumorigenic processes and was closely associated with HCC tumor cell growth, metastasis, or invasion, thereby making the four-gene signature construct a powerful biomarker for the prediction of HCC prognosis.

Evaluation of the four-gene construct using GSEA showed certain significantly enriched tumor features and various metabolic features. The analysis revealed that a large number of tumor-related pathways were significantly overexpressed in subtype C1, suggesting that the tumors of this subtype are more aggressive. This finding is also consistent with the clinical features of the tumors of C1 subtype such as late stage tumor, high degree of differentiation, and high mortality. On the other hand, the expression levels of metabolism-related pathways were higher in the C2 subtype compared to C1, and most of these metabolic pathways were related to physiological hepatocyte metabolic functions such as fatty acid metabolism, PPAR signaling pathway, and drug metabolic processes. This indicates a more intact hepatocyte function, thereby contributing to a better clinical outcome compared to the C1 subtype. Besides, we found that the tumor-related pathways increased with increasing RiskScore, while the metabolism-related pathways decreased with increasing RiskScore, which indicates that RiskScores can help predict the prognosis of HCC and aid in better understanding the molecular mechanisms underlying HCC onset and progression.

Three published gene signatures of HCC were compared to demonstrate the superiority of our model. Using a four-gene signature marker (Zheng) [30], we obtained 149 pairs of HCC specimens from GEO and identified 98 DEGs between HCC and normal hepatic tissues. Subsequently, we established and validated a four-gene subset of prognostic gene expression signature markers for HCC (*SPINK1*, *TXNRD1*, *LCAT*, and *PZP*). We found that the expression panel of these four genes strongly correlated with the methylation status of the genes. Another six-gene signature (Ke) marker [31] helped identify two prognostic molecular subtypes of HCC with different expression profiles and clinical outcomes. It also helped establish a prognostic evaluation model that not only distinguished the different subtypes of HCC, but also provided a good evaluation of patient prognosis. Another six-gene signature (Liu) marker [32], which included *CSE1L*, *CSTB*, *MTHFR*, *DAGLA*, *MMP10*, and *GYS2*, helped classify HCC patients into high- and low-risk groups with significant differences in their survival rates.

ROC analysis of the four models showed that the 5-year AUC values of the four-gene signature (Zheng), six-gene signature (Ke), and six-gene signature (Liu) markers were lower than that obtained in our model, indicating that our model is more reasonable and effective with similar number of genes. Besides, the C-index values of our RiskScore model were higher than those of the other three models, proving the good performance of our model.

Researchers have identified several genetic markers associated with cancer immunotherapy responsiveness, such as PD-L1 expression, tumor mutation burden (TMB), and DNA mismatch repair defects [69–71]. In 2020, the NCCN guidelines prioritized the use of atezolizumab and bevacizumab combination therapy [5]. However, the current use of immunotherapy for HCC is limited owing to the limited number of effective predictive markers [72, 73]. Therefore, we explored the ability of our four-gene model to predict immunotherapeutic efficacy by using an immunotherapy dataset (Imvigor210). We found that patients in the CR group had a significantly lower RiskScore compared to the PD group. We also found that higher RiskScore values were associated with poorer survival, and that the proportion of samples with immunotherapy response (CR + PR) was smaller in the high-risk group compared to the low-risk group (18% vs. 26%). In short, HCC patients from the high RiskScore group respond poorly to immunotherapy. However, this needs to be verified in the future via clinical trials.

Despite the promising findings obtained, our study has certain limitations. Firstly, our findings were based on a single platform and the study was retrospective. Data from different centers and different platforms are needed to further verify the performance of our model. Secondly, the limited sample size could have resulted in selection bias. Thirdly, our process of screening for differential genes was mainly based on statistics. Consequently, certain biologically significant genes may have been overlooked. Finally, the four genes identified in this study need to be subjected to more in-depth cellular experiments and animal studies to further explore their role in EMT, which will aid in laying the foundation for clinical applications.

## Conclusions

In this study, a four-gene signature (*PON1*, *FTCD*, *G6PD*, and *TMEM45A*) prognostic stratification system was constructed based on the EMT-associated genes of HCC cells, to effectively predict HCC prognosis. Additionally, the stability and accuracy of the model were evaluated. Our results reveal that the performance of our model is superior compared to that of the currently existing models. Therefore, through this study, we propose the use of

this classifier as a molecular diagnostic marker for the evaluation of the prognostic risk of patients with HCC.

## Abbreviations

EMT: Epithelial–mesenchymal transition; HCC: Hepatocellular carcinoma; DEGs: Differentially expressed genes; LIHC: Liver hepatocellular carcinoma; GEO: Gene Expression Omnibus; BSA: Bovine serum albumin; CR: Complete response; PD: Progressive disease; G6PD: Glucose-6-phosphate dehydrogenase; TMEM: Transmembrane protein.

## Supplementary Information

The online version contains supplementary material available at <https://doi.org/10.1186/s12935-021-02326-8>.

**Additional file 1: Table S1.** 59 EMT genes related to the prognosis of liver cancer

**Additional file 2: Table S2.** 1130 differentially expressed genes between molecular subtypes

**Additional file 3: Table S3.** 71 differentially expressed genes related to prognosis among molecular subtypes

## Acknowledgements

We thank Bullet Edits Limited for the linguistic editing and proofreading of the manuscript (<http://bulletedits.cn/>).

## Authors' contributions

XDF, WY, and WJC designed the study, performed data analysis, and wrote the manuscript. LSX, and CYH performed data collection, ZJF supervised the manuscript. All authors read and approved the final manuscript.

## Funding

This research was supported by Natural Science Foundation of Hainan Province Project (820MS130); Hainan Clinical Research Center for Malignant Tumors of Gastrointestinal System (LCYX202101).

## Availability of data and materials

The data used to support the findings of this study are available from the corresponding author on reasonable request.

## Declarations

### Ethics approval and consent to participate

The patients and their families in this study were fully informed, and informed consent was obtained from the participants. All research is conducted in accordance with the Helsinki Declaration. This study was approved by the Ethics Committee of Hainan General Hospital.

### Consent for publication

The current manuscript has been read and approved by all named authors.

### Competing interests

The authors declare that the research was conducted in the absence of any commercial or financial relationships that could be construed as a potential conflict of interest.

### Author details

<sup>1</sup>Department of Hepatobiliary and Pancreatic Surgery, Hainan General Hospital, Hainan Affiliated Hospital of Hainan Medical University, Haikou, Hainan, China. <sup>2</sup>Geriatric Medicine Center, Hainan General Hospital, Hainan Affiliated Hospital of Hainan Medical University, Haikou, Hainan, China.

Received: 15 July 2021 Accepted: 10 November 2021  
Published online: 24 November 2021

## References

- Díaz-González Á, Forner A, Lope C, Varela M. New challenges in clinical research on hepatocellular carcinoma. *Rev Esp Enferm Dig*. 2016;108(8):485–93.
- Chaisaingmongkol J, Budhu A, Dang H, Rabibhadana S, Pupacdi B, Kwon SM, Forgues M, Pomyen Y, Bhudhisawasdi V, Lertprasertsuke N, et al. Common Molecular Subtypes Among Asian Hepatocellular Carcinoma and Cholangiocarcinoma. *Cancer cell*. 2017;32(1):57–70.e53.
- Kulik L, El-Serag HB. Epidemiology and Management of Hepatocellular Carcinoma. *Gastroenterology*. 2019;156(2):477–491.e471.
- Sia D, Villanueva A, Friedman SL, Llovet JM. Liver cancer cell of origin, molecular class, and effects on patient prognosis. *Gastroenterology*. 2016;152(4):745.
- Benson AB, D'Angelica MI, Abbott DE, Anaya DA, Anders R, Are C, Bachini M, Borad M, Brown D, Burgoyne A, et al. Hepatobiliary cancers, version 2.2021, NCCN clinical practice guidelines in oncology. *J Natl Compr Canc Netw*. 2021;19(5):541–65.
- Anwanwan D, Singh SK, Singh S, Saikam V, Singh R. Challenges in liver cancer and possible treatment approaches. *Biochim Biophys Acta Rev Cancer*. 2020;1873(1):1883–14.
- Bruix J, Gores GJ, Mazzaferro V. Hepatocellular carcinoma: clinical frontiers and perspectives. *Gut*. 2014;63(5):844–55.
- El Dika I, Khalil DN, Abou-Alfa GK. Immune checkpoint inhibitors for hepatocellular carcinoma. *Cancer*. 2019;125(19):3312–9.
- Rasool M, Rashid S, Arooj M, Ansari SA, Khan KM, Malik A, Naseer MI, Zahid S, Manan A, Asif M, et al. New possibilities in hepatocellular carcinoma treatment. *Anticancer Res*. 2014;34(4):1563–71.
- Ogunwobi OO, Harricharran T, Huaman J, Galuza A, Odumuwaqun O, Tan Y, Ma GX, Nguyen MT. Mechanisms of hepatocellular carcinoma progression. *World J Gastroenterol*. 2019;25(19):2279–93.
- Chen T, You Y, Jiang H, Wang ZZ. Epithelial-mesenchymal transition (EMT): a biological process in the development, stem cell differentiation, and tumorigenesis. *J Cell Physiol*. 2017;232(12):3261–72.
- Zhang Y, Weinberg RA. Epithelial-to-mesenchymal transition in cancer: complexity and opportunities. *Front Med*. 2018;12(4):361–73.
- Ye X, Weinberg RA. Epithelial-mesenchymal plasticity: a central regulator of cancer progression. *Trends Cell Biol*. 2015;25(11):675–86.
- Tiwari N, Gheldof A, Tatarì M, Cristofori G. EMT as the ultimate survival mechanism of cancer cells. *Semin Cancer Biol*. 2012;22(3):194–207.
- Giannelli G, Koudelkova P, Dituri F, Mikulits W. Role of epithelial to mesenchymal transition in hepatocellular carcinoma. *J Hepatol*. 2016;65(4):798–808.
- Gurusu S, Kobori L, Fodor D, Jung I. Epithelial mesenchymal and endothelial mesenchymal transitions in hepatocellular carcinoma: a review. *Biomed Res Int*. 2019;2019:2962580.
- Guo F, Wang H, Jiang M, Yang Q, Xiang Q, Zhou H, Hu X, Hao K, Yang J, Cao H, et al. TDP-43 induces EMT and promotes hepatocellular carcinoma metastasis via activating Wnt/ $\beta$ -catenin signaling pathway. *Am J Cancer Res*. 2020;10(10):3285–301.
- Yang Y, Zhang N, Zhu J, Hong XT, Liu H, Ou YR, Su F, Wang R, Li YM, Wu Q. Downregulated connexin32 promotes EMT through the Wnt/ $\beta$ -catenin pathway by targeting Snail expression in hepatocellular carcinoma. *Int J Oncol*. 2017;50(6):1977–88.
- Yang M, Li SN, Anjum KM, Gui LX, Zhu SS, Liu J, Chen JK, Liu QF, Ye GD, Wang WJ, et al. A double-negative feedback loop between Wnt- $\beta$ -catenin signaling and HNF4 $\alpha$  regulates epithelial-mesenchymal transition in hepatocellular carcinoma. *J Cell Sci*. 2013;126(Pt 24):5692–703.
- Huang M, Wu S, Hu Q, Wu H, Wei S, Xie H, Sun K, Li X, Fang L. Agkhipin, a novel SVAE may inhibit the migration and invasion of liver cancer cells associated with the inversion of EMT induced by Wnt/ $\beta$ -catenin signaling inhibition. *Biochem Biophys Res Commun*. 2016;479(2):283–9.
- Zhang Q, Bai X, Chen W, Ma T, Hu Q, Liang C, Xie S, Chen C, Hu L, Xu S, et al. Wnt/ $\beta$ -catenin signaling enhances hypoxia-induced epithelial-mesenchymal transition in hepatocellular carcinoma via crosstalk with hif-1 $\alpha$  signaling. *Carcinogenesis*. 2013;34(5):962–73.
- Xia L, Huang W, Tian D, Zhu H, Qi X, Chen Z, Zhang Y, Hu H, Fan D, Nie Y, et al. Overexpression of forkhead box C1 promotes tumor metastasis and indicates poor prognosis in hepatocellular carcinoma. *Hepatology*. 2013;57(2):610–24.
- Yang MH, Chen CL, Chau GY, Chiou SH, Su CW, Chou TY, Peng WL, Wu JC. Comprehensive analysis of the independent effect of twist and snail in promoting metastasis of hepatocellular carcinoma. *Hepatology*. 2009;50(5):1464–74.
- Zeng B, Lin Z, Ye H, Cheng D, Zhang G, Zhou J, Huang Z, Wang M, Cai C, Zeng J, et al. Upregulation of LncDQ is associated with poor prognosis and promotes tumor progression via epigenetic regulation of the EMT pathway in HCC. *Cell Physiol Biochem*. 2018;46(3):1122–33.
- Mir N, Jayachandran A, Dhungel B, Shrestha R, Steel JC. Epithelial-to-mesenchymal transition: a mediator of sorafenib resistance in advanced hepatocellular carcinoma. *Curr Cancer Drug Targets*. 2017;17(8):698–706.
- Chen X, Lingala S, Khoobyari S, Nolte J, Zern MA, Wu J. Epithelial mesenchymal transition and hedgehog signaling activation are associated with chemoresistance and invasion of hepatoma subpopulations. *J Hepatol*. 2011;55(4):838–45.
- Chow AK, Ng L, Lam CS, Wong SK, Wan TM, Cheng NS, Yau TC, Poon RT, Pang RW. The enhanced metastatic potential of hepatocellular carcinoma (HCC) cells with sorafenib resistance. *PLoS ONE*. 2013;8(11):e78675.
- Nagai T, Arai T, Furuta K, Sakai K, Kudo K, Kaneda H, Tamura D, Aomatsu K, Kimura H, Fujita Y, et al. Sorafenib inhibits the hepatocyte growth factor-mediated epithelial mesenchymal transition in hepatocellular carcinoma. *Mol Cancer Ther*. 2011;10(1):169–77.
- Thorsson V, Gibbs DL, Brown SD, Wolf D, Bortone DS, Ou Yang TH, Porta-Pardo E, Gao GF, Plaisier CL, Eddy JA, et al. The immune landscape of cancer. *Immunity*. 2018;48(4):812–830.e814.
- Zheng Y, Liu Y, Zhao S, Zheng Z, Shen C, An L, Yuan Y. Large-scale analysis reveals a novel risk score to predict overall survival in hepatocellular carcinoma. *Cancer Manag Res*. 2018;10:6079–96.
- Ke K, Chen G, Cai Z, Huang Y, Zhao B, Wang Y, Liao N, Liu X, Li Z, Liu J. Evaluation and prediction of hepatocellular carcinoma prognosis based on molecular classification. *Cancer Manag Res*. 2018;10:5291–302.
- Liu GM, Zeng HD, Zhang CY, Xu JWJCC. Identification of a six-gene signature predicting overall survival for hepatocellular carcinoma. 2019;19(1).
- Sayiner M, Golabi P, Younossi ZM. Disease burden of hepatocellular carcinoma: a global perspective. *Dig Dis Sci*. 2019;64(4):910–7.
- Mackness M, Mackness B. Human paraoxonase-1 (PON1): gene structure and expression, promiscuous activities and multiple physiological roles. *Gene*. 2015;567(1):12–21.
- Bacchetti T, Ferretti G, Sahebkar A. The role of paraoxonase in cancer. *Semin Cancer Biol*. 2019;56:72–86.
- Kotur-Stevuljevic J, Vekic J, Stefanovic A, Zeljkovic A, Ninic A, Ivanisevic J, Miljkovic M, Sopic M, Munjas J, Mihajlovic M, et al. Paraonase 1 and atherosclerosis-related diseases. *BioFactors*. 2020;46(2):193–205.
- Arenas M, Rodriguez E, Sahebkar A, Sabater S, Rizo D, Pallise O, Hernandez M, Riu F, Camps J, Joven J. Paraonase-1 activity in patients with cancer: a systematic review and meta-analysis. *Crit Rev Oncol Hematol*. 2018;127:6–14.
- Liu P, Wang Q, Cui Y, Wang J. A meta-analysis of the relationship between paraoxonase 1 polymorphisms and cancer. *Free Radic Res*. 2019;53(11–12):1045–50.
- Saadat M. Paraonase 1 genetic polymorphisms and susceptibility to breast cancer: a meta-analysis. *Cancer Epidemiol*. 2012;36(2):e101–103.
- Dowling P, Hayes C, Ting KR, Hameed A, Meiller J, Mitsiades C, Anderson KC, Clynes M, Clarke C, Richardson P, et al. Identification of proteins found to be significantly altered when comparing the serum proteome from multiple myeloma patients with varying degrees of bone disease. *BMC Genom*. 2014;15:904.
- Afsar CU, Gunaldi M, Okuturlar Y, Gedikbasi A, Tiken EE, Kahraman S, Karaca F, Ercolak V, Karabulut M. Paraonase-1 and arylesterase activities in patients with colorectal cancer. *Int J Clin Exp Med*. 2015;8(11):21599–604.
- Arenas M, Garcia-Heredia A, Cabre N, Luciano-Mateo F, Hernandez-Aguilera A, Sabater S, Bonet M, Gascon M, Fernandez-Arroyo S, Fort-Gallifa I, et al. Effect of radiotherapy on activity and concentration of serum paraonase-1 in breast cancer patients. *PLoS ONE*. 2017;12(11):e0188633.
- Rodriguez-Tomas E, Murcia M, Arenas M, Arguis M, Gil M, Amigo N, Correig X, Torres L, Sabater S, Baiges-Gaya G, et al. Serum paraonase-1-related variables and lipoprotein profile in patients with lung or head and neck cancer: effect of radiotherapy. *Antioxidants*. 2019;8(7).
- Cao X, Cao Z, Shao Y, Liu C, Yan G, Meng X, Zhang L, Chen C, Huang G, Shu H, et al. Analysis of serum paraonase 1 using mass spectrometry and lectin immunoassay in patients with alpha-fetoprotein negative hepatocellular carcinoma. *Front Oncol*. 2021;11:651421.

45. Zhang S, Jiang K, Zhang Q, Guo K, Liu Y. Serum fucosylated paraoxonase 1 as a potential glyco-biomarker for clinical diagnosis of early hepatocellular carcinoma using ELISA Index. *Glycoconj J*. 2015;32(3–4):119–25.
46. Akkiz H, Kuran S, Akgollu E, Uskudar O, Bekar A, Bayram S, Yildirim S, Ulger Y, Kaya BY, Sansal M, et al. Effect of PON1 gene polymorphisms in Turkish patients with hepatocellular carcinoma. *Meta Gene*. 2013;1:93–101.
47. Yu Z, Ou Q, Chen F, Bi J, Li W, Ma J, Wang R, Huang X. Evaluation of the prognostic value of paraoxonase 1 in the recurrence and metastasis of hepatocellular carcinoma and establishment of a liver-specific predictive model of survival. *J Transl Med*. 2018;16(1):327.
48. Shu H, Li W, Shang S, Qin X, Zhang S, Liu Y. Diagnosis of AFP-negative early-stage hepatocellular carcinoma using Fuc-PON1. *Discov Med*. 2017;23(126):163–8.
49. Ding GY, Zhu XD, Ji Y, Shi GM, Shen YH, Zhou J, Fan J, Sun HC, Huang C. Serum PON1 as a biomarker for the estimation of microvascular invasion in hepatocellular carcinoma. *Ann Transl Med*. 2020;8(5):204.
50. Huang C, Wang Y, Liu S, Ding G, Liu W, Zhou J, Kuang M, Ji Y, Kondo T, Fan J. Quantitative proteomic analysis identified paraoxonase 1 as a novel serum biomarker for microvascular invasion in hepatocellular carcinoma. *J Proteome Res*. 2013;12(4):1838–46.
51. Kohls D, Sulea T, Purisima EO, MacKenzie RE, Vrieland A. The crystal structure of the formiminotransferase domain of formiminotransferase-cyclodeaminase: implications for substrate channeling in a bifunctional enzyme. *Structure*. 2000;8(1):35–46.
52. Chen J, Chen Z, Huang Z, Yu H, Li Y, Huang W. Formiminotransferase cyclodeaminase suppresses hepatocellular carcinoma by modulating cell apoptosis, DNA damage, and phosphatidylinositol 3-kinases (PI3K)/Akt signaling pathway. *Med Sci Monit*. 2019;25:4474–84.
53. Seimiya M, Tomonaga T, Matsushita K, Sunaga M, Oh-Ishi M, Kodera Y, Maeda T, Takano S, Togawa A, Yoshitomi H, et al. Identification of novel immunohistochemical tumor markers for primary hepatocellular carcinoma: clathrin heavy chain and formiminotransferase cyclodeaminase. *Hepatology*. 2008;48(2):519–30.
54. Labib OH, Harb OA, Khalil OH, Baiomy TA, Gertallah LM, Ahmed RZ. The diagnostic value of arginase-1, FTCD, and MOC-31 expression in early detection of hepatocellular carcinoma (HCC) and in differentiation between HCC and metastatic adenocarcinoma to the liver. *J Gastrointest Cancer*. 2020;51(1):88–101.
55. Kanarek N, Keys HR, Cantor JR, Lewis CA, Chan SH, Kunchok T, Abu-Remaileh M, Freinkman E, Schweitzer LD, Sabatini DM. Histidine catabolism is a major determinant of methotrexate sensitivity. *Nature*. 2018;559(7715):632–6.
56. Luzzatto L, Ally M, Notaro R. Glucose-6-phosphate dehydrogenase deficiency. *Blood*. 2020;136(11):1225–40.
57. Zhang C, Zhang Z, Zhu Y, Qin S. Glucose-6-phosphate dehydrogenase: a biomarker and potential therapeutic target for cancer. *Anticancer Agents Med Chem*. 2014;14(2):280–9.
58. Yang HC, Wu YH, Yen WC, Liu HY, Hwang TL, Stern A, Chiu DT. The redox role of G6PD in cell growth, cell death, and cancer. *Cells*. 2019;8(9).
59. Ghergurovich JM, Esposito M, Chen Z, Wang JZ, Bhatt V, Lan T, White E, Kang Y, Guo JY, Rabinowitz JD. Glucose-6-phosphate dehydrogenase is not essential for K-Ras-driven tumor growth or metastasis. *Cancer Res*. 2020;80(18):3820–9.
60. Mele L, la Noce M, Paino F, Regad T, Wagner S, Liccardo D, Papaccio G, Lombardi A, Caraglia M, Tirino V, et al. Glucose-6-phosphate dehydrogenase blockade potentiates tyrosine kinase inhibitor effect on breast cancer cells through autophagy perturbation. *J Exp Clin Cancer Res*. 2019;38(1):160.
61. Li R, Wang W, Yang Y, Gu C. Exploring the role of glucose-6-phosphate dehydrogenase in cancer (Review). *Oncol Rep*. 2020;44(6):2325–36.
62. Barajas JM, Reyes R, Guerrero MJ, Jacob ST, Motiwala T, Ghoshal K. The role of miR-122 in the dysregulation of glucose-6-phosphate dehydrogenase (G6PD) expression in hepatocellular cancer. *Sci Rep*. 2018;8(1):9105.
63. Schmit K, Michiels C. TMEM proteins in cancer: a review. *Front Pharmacol*. 2018;9:1345.
64. Manawapat-Klopfer A, Thomsen LT, Martus P, Munk C, Russ R, Gmuender H, Frederiksen K, Haedicke-Jarboui J, Stubenrauch F, Kjaer SK, et al. TMEM45A, SERPINB5 and p16INK4A transcript levels are predictive for development of high-grade cervical lesions. *Am J Cancer Res*. 2016;6(7):1524–36.
65. Sun W, Qiu G, Zou Y, Cai Z, Wang P, Lin X, Huang J, Jiang L, Ding X, Hu G. Knockdown of TMEM45A inhibits the proliferation, migration and invasion of glioma cells. *Int J Clin Exp Pathol*. 2015;8(10):12657–67.
66. Guo J, Chen L, Luo N, Yang W, Qu X, Cheng Z. Inhibition of TMEM45A suppresses proliferation, induces cell cycle arrest and reduces cell invasion in human ovarian cancer cells. *Oncol Rep*. 2015;33(6):3124–30.
67. Flamant L, Roegiers E, Pierre M, Hayez A, Sterpin C, De Backer O, Arnould T, Poumay Y, Michiels C. TMEM45A is essential for hypoxia-induced chemoresistance in breast and liver cancer cells. *BMC Cancer*. 2012;12:391.
68. Zhu M, Jiang B, Yan D, Wang X, Ge H, Sun Y. Knockdown of TMEM45A overcomes multidrug resistance and epithelial–mesenchymal transition in human colorectal cancer cells through inhibition of TGF- $\beta$  signaling pathway. *Clin Exp Pharmacol Physiol*. 2020;47(3):503–16.
69. Fridman WH, Zitvogel L, Sautes-Fridman C, Kroemer G. The immune contexture in cancer prognosis and treatment. *Nat Rev Clin Oncol*. 2017;14(12):717–34.
70. Hodges TR, Ott M, Xiu J, Gatalica Z, Swensen J, Zhou S, Huse JT, de Groot J, Li S, Overwijk WW, et al. Mutational burden, immune checkpoint expression, and mismatch repair in glioma: implications for immune checkpoint immunotherapy. *Neuro Oncol*. 2017;19(8):1047–57.
71. Yarchoan M, Hopkins A, Jaffee EM. Tumor mutational burden and response rate to PD-1 inhibition. *N Engl J Med*. 2017;377(25):2500–1.
72. Johnston MP, Khakoo SI. Immunotherapy for hepatocellular carcinoma: current and future. *World J Gastroenterol*. 2019;25(24):2977–89.
73. Xu F, Jin T, Zhu Y, Dai C. Immune checkpoint therapy in liver cancer. *J Exp Clin Cancer Res*. 2018;37(1):110.

## Publisher's Note

Springer Nature remains neutral with regard to jurisdictional claims in published maps and institutional affiliations.

Ready to submit your research? Choose BMC and benefit from:

- fast, convenient online submission
- thorough peer review by experienced researchers in your field
- rapid publication on acceptance
- support for research data, including large and complex data types
- gold Open Access which fosters wider collaboration and increased citations
- maximum visibility for your research: over 100M website views per year

At BMC, research is always in progress.

Learn more [biomedcentral.com/submissions](https://biomedcentral.com/submissions)

